T. C.
Inonu University
Graduate School of Nature and Applied Sciences

WOUND HEALING METHOD WITH LORENTZ FIELDS: NUMERICAL STUDIES AND ANIMAL EXPERIMENTS

Master of Thesis

ALİYE GÜRCAN

Department of Biomedical Engineering

Thesis Supervisor: Asst. Prof. Dr. Reyhan ZENGİN

November 2024

T.C.
Inonu University
Graduate School of Nature and Applied Sciences

WOUND HEALING METHOD WITH LORENTZ FIELDS: NUMERICAL STUDIES AND ANIMAL EXPERIMENTS

Master of Thesis

ALİYE GÜRCAN
36203630073

Department of Biomedical Engineering

Thesis Supervisor: Asst. Prof. Dr. Reyhan ZENGİN
November 2024

ACKNOWLEDGMENTS AND FOREWORD

I would like to express my deepest gratitude to Asst. Prof. Dr. Reyhan Zengin for her guidance, advice, help, and support. Her understanding and patience during my thesis study made this thesis process possible.

I would also like to thank my family for their understanding and support throughout my education.

I would like to express my gratitude to my dear husband Mücahit for his love and support under all circumstances.

I would like to thank my friends Rabia Tutuk and Elif Feyza Aydın for their support during my thesis, especially at the end of the animal experiments part of our study.

I would like to express my sincere thanks to TUBITAK for their support, which made a great contribution to the realization of this study. The financial support and research facilities provided to my TUBITAK 1001 project coded 122E150 played a vital role in the successful completion of this study. I would like to thank all TUBITAK staff for guiding me through this process. I would like to thank Prof. Dr. Suat Tekin and Assoc. Prof. Dr. Çiğdem Tekin for their support in the data analysis part of the animal experiments study.

WORD of HONOR

I proudly confirm that this work titled ”WOUND HEALING METHOD WITH LORENTZ FIELDS: NUMERICAL STUDIES AND ANIMAL EXPERIMENTS,” which I submitted as a master’s thesis, was written by me without resorting to any help that would be contrary to scientific morals and traditions and that all the sources I have used are those shown following the method both in the text and in the bibliography.

ALİYE GÜRCAN

Table of Content

ACKNOWLEDGMENTS AND FOREWORD i

WORD of HONOR ii

INDEX OF SYMBOLS AND ABBREVIATIONS xi

ABSTRACT xii

ÖZET xiii

1 INTRODUCTION 1

1.1 Wound . . . 1
1.2 Chronic Wounds . . . 3
1.3 Wound (Injury) Current . . . 4
1.4 Surgical Wound Healing Method . . . 5
1.5 Non-surgical Wound Healing Methods . . . 6
1.5.1 Wound healing with electrical stimulation . . . 7
1.5.2 Wound healing method using ultrasound . . . 9
1.5.3 Wound healing using static magnetic field . . . 11
1.6 Objectives of the thesis . . . 12
1.7 Thesis Outline . . . 13

2 MATHEMATICAL BACKGROUND 14

2.1 Electromagnetic Field Equations . . . 14
2.2 Basic Acoustic Field Equations . . . 15

3 NUMERICAL MODELING 19

3.1 Model Geometry . . . 19
3.2 Ultrasonic Transducer . . . 19
3.3 Skin and Wound Modeling . . . 20
3.4 Pressure Acoustic Module . . . 22
3.5 Piezoelectric Module . . . 24
3.6 Electromagnetic Module . . . 26
3.7 Numerical Studies Results . . . 28
3.7.1 Transducer excitation . . . 28
3.7.2 Single Element model results . . . 30
3.7.3 Results from different steering angles . . . 31
3.7.4 Results from different focusing angles . . . 38

4 STUDIES OF ANIMAL EXPERIMENTS **41**
4.1 Preparation for Experimental Studies 41
4.1.1 Static magnetic field 42
4.1.2 Ultrasonic transducer 45
4.1.3 Lorentz Fields 46
4.2 Results of Animal Experiments 47

5 DISCUSSION AND CONCLUSION **60**

RESUME **74**

List of Tables

Table 3.1 : Parameters used in the model, including electrical conductivity (at 1 MHz frequency), density, and speed of sound for different tissue types [72–75]. **22**

Table 3.2 : Current density distribution in the center of the wound region of a 16-element LPA transducer driven by a 100 V signal between -30 and $+30$ steering angles. **38**

Table 3.3 : The absolute value distribution of the current density in the center of the winding region is focused by a 16-element LPA converter driven by a 100 V signal. **40**

Table 5.1 : Stimulation parameters having similar effects [104]. **64**

List of Figures

Figure 1.1 : Wound types, skin structure, and wound healing phases. **a** Different wound types, **b** The skin structure consists of three layers: the epidermis, dermis, and hypodermis. **c** The phase of wound healing includes hemostasis, inflammation, proliferation, and tissue remodeling [87]. **3**

Figure 3.1 : Specifications of the 16-Element LPA Ultrasonic Transducer. [86] **20**

Figure 3.2 : LPA Wound Model in Comsol Multiphysics. The model defines the ultrasonic transducer, air, wound, skin layers, and skin dimensions. **21**

Figure 3.3 Single Element Wound Model in Comsol Multiphysics. The model defines the ultrasonic transducer, air, wound, skin layers, and skin dimensions. **21**

Figure 3.4 : Geometry of the pressure acoustic problem. Subdomains Ω_1, Ω_2, Ω_3, Ω_4, Ω_5, Ω_6, Ω_7 and associated boundaries $\partial\Omega_1$, $\partial\Omega_2$, $\partial\Omega_3$, $\partial\Omega_4$, $\partial\Omega_5$, $\partial\Omega_6$ and $\partial\Omega_7$ represent the ultrasonic gel, epidermis, dermis, hypodermis, wound, ultrasonic transducer and air, respectively. **23**

Figure 3.5 : p Geometry for the piezoelectric module. Subdomains Ω_1, Ω_2, Ω_3, Ω_4, Ω_6, Ω_7 and associated boundaries $\partial\Omega_1$, $\partial\Omega_2$, $\partial\Omega_3$, $\partial\Omega_4$, $\partial\Omega_6$ and $\partial\Omega_7$ represent the ultrasonic gel, epidermis, dermis, hypodermis, ultrasonic transducer and air, respectively. $\partial\Omega_6$ represents the surface of the crystal where the voltage is applied. On $\partial\Omega_9$ and $\partial\Omega_10$ the assumption is made that the normal component of the electrical displacement is zero. The boundary $\partial\Omega_8$ acts as the electrical ground in the problem. . . . **25**

Figure 3.6 : Geometry of the electromagnetic problem. Subdomains Ω_1, Ω_2, Ω_3, Ω_4, Ω_5, Ω_7 and associated boundaries $\partial\Omega_1$, $\partial\Omega_2$, $\partial\Omega_3$, $\partial\Omega_4$, $\partial\Omega_5$ and $\partial\Omega_7$ represent the ultrasonic gel, epidermis, dermis, hypodermis and air, respectively. **27**

Figure 3.7 Applied voltage (V) to each piezoelectric crystal. The amplitude of the electrical signal is selected as 1 V as given in the y-axis. The x-axis shows time in seconds [69]. **29**

Figure 3.8 **a)** Current density and **b)** pressure distribution in the wound area for a Single-Element transducer driven with a 100 V signal (t = 8 μs). **30**
Figure 3.9 **a)** Current density and **b)** pressure distribution in the middle of the wound area for a Single-Element transducer driven with a 100 V signal (t = 4 μs). **30**
Figure 3.10 **a)** Current density and **b)** pressure distribution in the middle of the wound area for a 16-element LPA transducer driven with a 100 V signal (t = 4 μs). **31**
Figure 3.11 Current density (**a, c**) and pressure (**b, d**) distributions in the middle of the wound area for a 16-element LPA transducer driven with 100 V and a full signal (t = 4 μs) at -5 degree (**a, b**) and $+5$ degree (**c, d**) orientations. **32**
Figure 3.12 Current density (**a, c**) and pressure (**b, d**) distributions in the middle of the wound area for a 16-element LPA transducer driven with 100 V and a full signal (t = 4 μs) at -10 degree (**a, b**) and $+10$ degree (**c, d**) orientations. **33**
Figure 3.13 Current density (**a, c**) and pressure (**b, d**) distributions in the middle of the wound area for a 16-element LPA transducer driven with 100 V and a full signal (t = 4 μs) at -15 degree (**a, b**) and $+15$ degree (**c, d**) orientations. **34**
Figure 3.14 Current density (**a, c**) and pressure (**b, d**) distributions in the middle of the wound area for a 16-element LPA transducer driven with 100 V and a full signal (t = 4 μs) at -20 degree (**a, b**) and $+20$ degree (**c, d**) orientations. **35**
Figure 3.15 Current density (**a, c**) and pressure (**b, d**) distributions in the middle of the wound area for a 16-element LPA transducer driven with 100 V and a full signal (t = 4 μs) at -25 degree (**a, b**) and $+25$ degree (**c, d**) orientations. **36**
Figure 3.16 Current density (**a, c**) and pressure (**b, d**) distributions in the middle of the wound area for a 16-element LPA transducer driven with 100 V and a full signal (t = 4 μs) at -30 degree (**a, b**) and $+30$ degree (**c, d**) orientations. **37**
Figure 3.17 **a)** Pressure distribution and **b)** current density in the center of the wound area when a 100 V signal is applied using two crystals of a 16-element LPA transducer (t=4 μs). **39**

Figure 3.18 **a)** Pressure distribution and **b)** current density in the center of the wound area when a 100 V signal is applied using four crystals of a 16-element LPA transducer (t=4 μs). **39**
Figure 3.19 **a)** Pressure distribution and **b)** current density in the center of the wound area when a 100 V signal is applied using six crystals of a 16-element LPA transducer (t=4 μs). **40**
Figure 4.1 **:** Experiment setup photo. The DC power supply powers the Helmholtz coils. Helmholtz coils and magnets are used to generate a static magnetic field. An RF amplifier and a waveform generator drive an ultrasonic transducer to generate acoustic pressure. **41**
Figure 4.2 **:** Helmholtz coil pairs model with DC power supply and a Tesla meter. **42**
Figure 4.3 **:** Variation of Magnetic Field on the Central Axis according to Distance [99]. **43**
Figure 4.4 **:** Measurement of static magnetic fields utilizing Helmholtz coils with Gaussmeter. **43**
Figure 4.5 **:** Line graph of magnetic flux density for each permanent magnet pair between the magnets **44**
Figure 4.6 **:** Permanent Magnets Measurements. a) Nearby the left magnet. The magnetic flux density is 421.4 mTesla. b) At the center of magnets. The magnetic flux density is 123.3 mTesla. c) Nearby the right magnet. Magnetic flux density is 420.7 mTesla. **44**
Figure 4.7 **:** Ultrasonic Experiment Model. a)RF amplifier, Waveform Generator, and Oscilloscope measurements. b) A single-element immersion transducer, Olympus Accuscan A303S-SU. **45**
Figure 4.8 **:** Lorentz Field Experiment Model. It consists of permanent magnets and an ultrasonic transducer. **46**
Figure 4.9 **:** Stages of skin wound formation in rats used in the study. a) Shaving the selected area of the rat for the wound. b) Applying povidone iodine to the wound site of a rat. c) Cleaning the wound site of the rat with ethyl alcohol. d) Determination of the wound area generated by measuring with a ruler. e) Cutting the wound area after measurement. f) Image of the wound generated. **48**

Figure 4.10 : Cages housing the rats (n=31) and the rack on which the cages are placed. a) Static Magnetic Field group (n=8), b) Ultrasound group (n=8), c) Lorentz Field group (n=8), d) Control group (n=7). **49**
Figure 4.11 : Application with permanent magnets. a) Measurement of the magnetic field at the right edge of the magnet during the application. b) Measurement of the magnetic field at the center of the setup during the application. **49**
Figure 4.12 : Application with Helmholtz coils. **50**
Figure 4.13 : Application with Ultrasound. (a) Ultrasound gel was applied to the transducer. (b) Contact of the ultrasound gel with the wound surface. (c) Application of ultrasound method to the rat. **51**
Figure 4.14 : Application of Lorentz Field method to the rat. **52**
Figure 4.15 : After the wound was generated, measurements were done and photographed on the wounds of the rats in all groups during the 14-day application period. **54**
Figure 4.16 : Wound measurements for all groups over the 14-day application period following wound formation. The table records the short side (ss) and long side (ls) dimensions of the wounds. **56**
Figure 4.17 On the first day, wound healing rates in all groups were similar at baseline. There was no significant difference in long side (ls) (a) and short side (ss) (b) measurements, and no statistically significant difference was observed between the groups at the beginning of the healing process. **57**
Figure 4.18 Sixth day analyses showed a significant improvement in the healing rates of Lorentz Field (LF) and Ultrasound (US) groups compared to the control and Static Magnetic Field (SMF) groups (*$p<0.05$). It was observed that the healing rate increased in both long side and short side measurements in LF and US groups. This indicates that LF and US applications may accelerate wound healing. **58**

Figure 4.19 Between days 6-9, a statistically significant decrease in short side (ss) measurements was observed especially in the LF group (*p$<$0.05, indicating that the recovery rate was faster compared to the control and SMF groups. Although a similar trend was observed in the US group, a lower effect was observed compared to the LF group. In the SMF group, a slight improvement was observed compared to the control group, but this difference was not significant. **58**

Figure 4.20 The LF group showed the highest healing rate between the 9th and 15th days (*p$<$0.05 and a significant reduction was observed especially in the short side (ss) values. The US group also continued to heal during this period, but showed a lower effect than the LF group. The SMF group tends to improve, although it does not make a statistically significant difference compared to the control group. **59**

Figure 4.21 During the entire experimental period (days 1-15), statistically significant improvement was observed in the short side and long side measurements in the LF group (*p$<$0.05), while the US group showed a lower but significant improvement compared to the LF group. These results suggest that LF application may be an effective method in wound healing and US may support this process. **59**

INDEX OF SYMBOLS AND ABBREVIATIONS

PM	:	Pathogenic Microorganisms
TEP	:	Transepidermal Potentials
ES	:	Electrical stimulation
DC	:	Direct current
PC	:	Pulsed current
LIDC	:	low-intensity direct current
MPC	:	Monophasic Pulsed Current
HVPC	:	high-voltage pulsed current
LVPC	:	low-voltage pulsed current
TENS	:	Transcutaneous Electrical Nerve Stimulation
FREMS	:	Frequency Rhythmic Electrical Modulation System
MIST	:	Mist Ultrasound Therapy
SMF	:	Static magnetic field
FDA	:	US Food and Drug Administration
PEMF	:	pulsed electromagnetic field
PRFE	:	Pulsed radio frequency energy
LPA	:	Linear Phased Array
RF	:	Radio Frequency
FEM	:	Finite Element Method
LF	:	Lorentz Field
US	:	Ultrasound

Master of Thesis

WOUND HEALING METHOD WITH LORENTZ FIELDS: NUMERICAL STUDIES AND ANIMAL EXPERIMENTS

ALİYE GÜRCAN

Inonu University
Graduate School of Nature and Applied Sciences
Department of Biomedical Engineering

74+xiii pages

2024

Thesis Supervisor: Asst. Prof. Dr. Reyhan ZENGİN

Wound healing has been and will continue to be an important problem throughout human history. This study proposes a novel approach with Lorentz fields to accelerate wound healing. This approach is based on electric field-based Lorentz fields generated over static magnetic fields induced by ultrasound. The research consists of numerical studies and animal experiments. In the numerical studies, a two-dimensional wound model was developed. In this model, acoustic pressure was applied at different angles and focusing methods, and the interactions of these pressures on the static magnetic field were analyzed. In animal experiments, the effects of static magnetic field, ultrasound, and the proposed hybrid Lorentz field method were observed. Both numerical and experimental studies show that this research presents important findings and has the potential to accelerate the wound healing process. The proposed method offers an alternative approach to traditional wound healing methods.

Keywords: Wound healing, Lorentz fields, Static magnetic field, Ultrasound, Linear phased array transducer, Single element transducer, animal experiments

Yüksek Lisans Tezi

LORENTZ ALANLARI ILE YARA IYILEŞTIRME YÖNTEMI: SAYISAL ÇALIŞMALAR VE HAYVAN DENEYLERI

ALİYE GÜRCAN

İnönü Üniversitesi
Fen Bilimleri Enstitüsü
Biyomedikal Mühendisliği Anabilim Dalı

74+xiii sayfa

2024

Tez Danışmanı : Dr. Öğrt. Üyesi Reyhan ZENGİN

Yara iyileştirme, insanlık tarihi boyunca önemli bir sorun olmuştur ve olmaya devam edecektir. Bu çalışmada, yara iyileşmesini hızlandırmak amacıyla Lorentz alanlar ile yeni bir yaklaşım önerilmektedir. Bu yaklaşım, ultrasonla indüklenen statik manyetik alanlar üzerinden oluşturulan elektrik alan tabanlı Lorentz alanlarına dayanmaktadır. Araştırma, sayısal çalışmalar ve hayvan deneylerinden oluşmaktadır. Sayısal çalışmalar kapsamında, iki boyutlu bir yara modeli geliştirilmiştir. Bu modelde, farklı açılarda ve odaklama yöntemleriyle akustik basınç uygulanmış ve bu basınçların statik manyetik alan üzerindeki etkileşimleri incelenmiştir. Hayvan deneylerinde ise, statik manyetik alan, ultrason ve önerilen hibrit yöntem olan Lorentz alan metodunun etkileri gözlemlenmiştir. Hem sayısal hem de deneysel çalışmalar, bu araştırmanın önemli bulgular sunduğunu ve yara iyileştirme sürecini hızlandırma potansiyeline sahip olduğunu göstermektedir. Önerilen yöntem, geleneksel yara iyileştirme yöntemlerine alternatif bir yaklaşım sunmaktadır.

Anahtar Kelimeler: Yara iyileştirme, Lorentz alanlar, Statik manyetik alan, Ultrason, Doğrusal faz dizili dönüştürücü, Tek elemanlı dönüştürücü, hayvan deneyleri

1. INTRODUCTION

1.1 Wound

A wound is the damage to the tissue caused by physical or chemical factors. Wounds are generally classified into three types. The first type is based on the integrity of the skin, which can be either open or closed. Different types of open wounds encompass abrasions, incisions, slashes, punctures, contusions, and gunshot wounds. Closed wounds are caused by a crush or explosion. The second type is based on contamination with pathogenic microorganisms (PM) and can be either clean or infected. A clean wound is characterized by the absence of PM, tissue loss, or infection. Infected wounds, on the other hand, are those that are contaminated with harmful microorganisms, leading to delayed healing. The third category is classified based on the duration of formation, which can be acute or chronic. Acute wounds generally heal within a specific time frame under normal conditions, while chronic wounds persist for longer than three months and may tend to reoccur [1].

Wound care is a practice that dates back to the earliest periods of human history. The primary objective in wound care is to expedite the restoration of tissue integrity, prevent infection, and alleviate pain as effectively as possible [2] [3] [44].

The healing process of all wounds adheres to fundamental principles [5]. This process initiates promptly after injury and progresses through a distinct sequence of three stages [6] [9], which are hemostasis-inflammation, proliferation, and maturation [7]:

(a) ***The Hemostasis and Inflammation Phase***: This phase begins approximately 15 minutes after the injury and typically lasts between 1 and 5 minutes [5]. Initially, the wound site fills with blood, initiating intense bleeding [1]. This initial phase of intense bleeding and vascular response sets the stage for the subsequent processes of hemostasis and inflammation. Histamine, released from mast cells within the wound area, triggers vasodilation and increases vascular permeability. Upon injury, leukocytes, monocytes, platelets, and plasma are released from the blood vessels and move toward the site of injury [5]. This process leads to the formation of a blood clot by platelets, effectively halting further bleeding. [8][9]. Platelets are crucial for both hemostasis and coagula-

tion [8]. The healing process begins with the release of growth factors from the alpha granules of platelets that are present within the clot [1]. Without these factors, severe bleeding persists, leading to delayed wound healing. During hemostasis, fibrin is formed and plays a crucial role in clot formation at the injury site. This process can lead to local inflammation characterized by redness, swelling (edema), and fever in the wound area [9]. Macrophages, derived from monocytes, play a crucial role in wound healing. In addition to combating and engulfing bacteria, they remove dead tissue and other types of white blood cells.

About 72 hours following an injury, the most abundant cells in the wound, macrophages, release cytokines, which play a significant role in the inflammatory phase. [5]. The inflammatory phase is affected by various internal and external factors, and if it becomes excessive or uncontrolled, it can delay healing and harm the tissue. Conversely, insufficient recruitment of immune cells can also impede the healing process [8]. Concurrently, the formation of new blood vessels begins. These vessels transport oxygenated blood to the wound, enhancing its nourishment. This accelerates the development of granulation tissue, typically starting around the fifth day. Adequate oxygen and nutrient supply to the tissue are crucial for initiating this stage [5].

(b) ***Proliferation Phase (5-14 days)***: It usually starts a few hours after the injury and lasts for weeks [9]. In this phase, the main activities include the formation of granulation tissue and new epithelium [10]. Granulation tissue gradually replaces the accumulated fluid in the wound area, which helps with cell growth. The newly formed epithelial tissue acts as a protective barrier against foreign substances and helps maintain fluid and electrolyte balance within the wound [9]. Macrophages play a crucial role by attracting fibroblasts to the scar tissue, where they migrate and initiate the production of collagen fibers. These collagen fibers are important for providing tensile strength to the wound. The entry of polysaccharides and mucoproteins into the wound generates a flexible structure and a solid bridge between the wound walls [5]. The dark pink color of the granulation tissue signifies an enhanced supply of oxygen and nutrients to the scar tissue. [9]. As collagen production reaches adequate levels, fibrob-

lasts gradually decrease in number within the wound. This phase concludes with the establishment of granulation and the onset of epithelialization [5].

(c) ***Maturation Phase (after the 14th day):*** Following the completion of the proliferation phase [1] the maturation phase can extend for years. Collagen fibers, densely formed at the wound's edges, remodel, and type III (soft) collagen turns into type I (hard) collagen. These collagen fibers bind the wound tightly together [5]. The wound gradually resembles normal tissue in the maturation phase as fibroblasts and macrophages are gradually eliminated [1]. The essential characteristic of this phase is the restructuring of collagen [5]. During remodeling, collagen is replaced, and fibrin is withdrawn. At this stage, the newly formed tissue can regain up to 80 percent of its original strength, showing reduced strength and density [1].

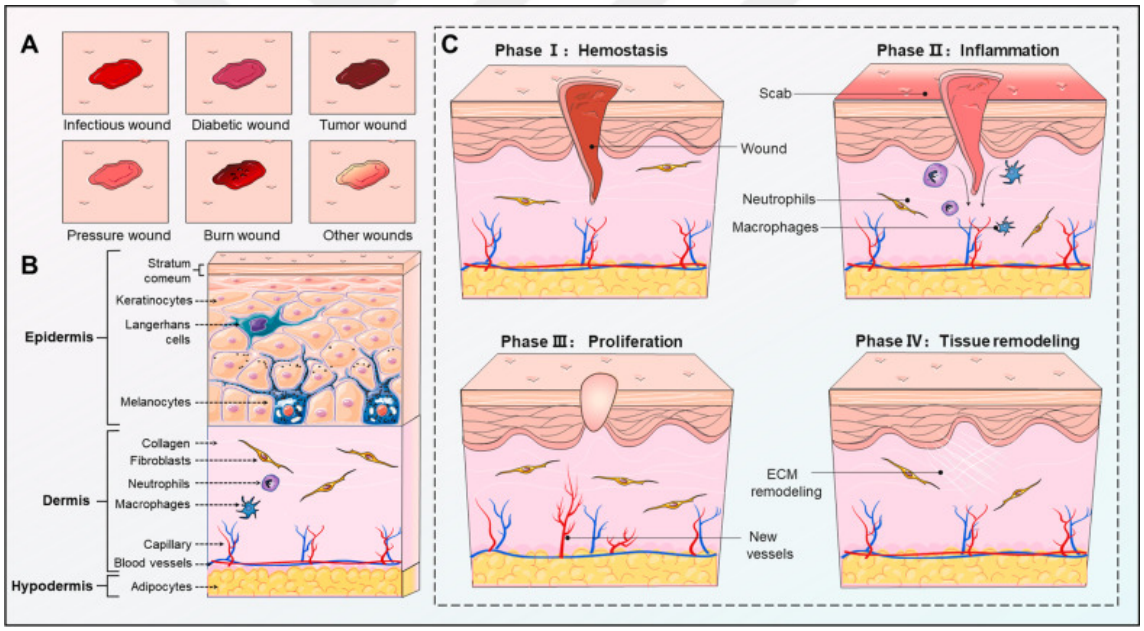


Figure 1.1 : Wound types, skin structure, and wound healing phases. **a** Different wound types, **b** The skin structure consists of three layers: the epidermis, dermis, and hypodermis. **c** The phase of wound healing includes hemostasis, inflammation, proliferation, and tissue remodeling [87].

1.2 Chronic Wounds

Chronic wounds, which require over 42 days to heal completely, present a major challenge for healthcare systems globally. In the United States, it results in an estimated cost of around 20 to 25 million dollars [11]. As the population ages, the

burden of chronic wounds is expected to rise, resulting in higher healthcare costs. One of the main factors contributing to the persistence of these wounds is severe inflammation in the scar tissue. Furthermore, chronic infections in the wounds can perpetuate this cycle, leading to ongoing inflammation and insufficient tissue repair. In particular, research shows that iron overload in wounds can further delay the healing process [10]. Various factors contribute to delayed wound healing, including diabetes, age, and vascular insufficiency [7]. These conditions generate an environment that impedes the body's natural healing mechanisms, prolonging the healing process and increasing the likelihood of chronicity. Addressing these factors and understanding the underlying mechanisms of chronic wounds are crucial steps in improving treatment outcomes and reducing the economic burden of these conditions.

1.3 Wound (Injury) Current

The concept of wound current was first introduced by Du Bois-Reymond in 1843. Reymond measured the wound current in the skin at 1 mA, forming the basis for subsequent studies with this measurement. Subsequent studies have shown that the electric current in wounds is less than 1 mA and that the electric field surrounding the wound constitutes an "injury current" [25]. Epithelial cells with Na+ and Cl- channels in the apical plasma membrane have Na+/K+ and ATPase in the basal plasma membrane. These ion channels with an asymmetrical distribution generate the current throughout the cell. Transepidermal potentials (TEP) are formed by the directional transport of ions in the wound. Studies have shown that this wound results from short-circuiting of the TEP [10] [26]. It has been observed that the injury current increases by 2-3 mm around the wound, and the electric field decreases from 140 mV/mm to 0 mV/mm [25]. Compared to the surrounding healthy tissue, the wound site acts as a cathode [10]. The current flowing through the wound pathway in the injured skin generates a lateral electric field. Therefore, injury current is thought to be necessary at the onset of repair of damaged tissue [7].

1.4 Surgical Wound Healing Method

Chronic wounds, especially those associated with diabetes, often resist conventional healing methods, necessitating advanced surgical interventions. Surgical interventions for chronic wounds are typically classified into three categories: negative pressure therapy, debridement, and mechanical closure. However, each approach carries its own set of complications, particularly in the case of diabetic ulcers. Negative pressure therapy, while often effective, can pose challenges in diabetic ulcers due to its bulkiness, which may be impractical in areas with limited space. Moreover, its effectiveness in diabetic ulcers is not well-established. Debridement, which involves the removal of dead tissue from wounds, can be painful for patients and may not optimally support the biological wound healing process, particularly in diabetic ulcers. The wound size may limit the use of closure techniques like sutures or staples and may not adequately facilitate wound healing, especially in diabetic ulcers. While these methods are generally effective in treating chronic wounds, they may not lead to favorable outcomes in elderly diabetic patients due to the specific challenges associated with their condition [12]. Hence, alternative strategies tailored to the specific needs of diabetic patients may be necessary to achieve optimal wound healing.

Negative pressure therapy, a non-invasive method, accelerates the healing of acute and chronic wounds through controlled pressure application [13] [21–23]. Its origins trace back to Fleischmann et al., who first introduced the concept of negative pressure application in treating open and infected wounds [14]. Over time, this method has become increasingly prevalent in managing acute and chronic wounds. The primary objective of negative pressure therapy is to maintain wound cleanliness, decrease infection and edema, enhance blood flow to the wound site, and promote granulation tissue development [15]. The procedure involves placing a sponge (vacuum) on the wound bed, from which fluids and other wound materials are drawn out via a hose. This process aids in removing infected tissue and fluid, thereby reducing the wound size. However, patients are typically required to remain attached to the vacuum apparatus for an extended duration [12]. In a study by Demir et al., negative pressure wound therapy was applied to 50 patients with chronic wounds for an average of 12.4 days. The results demonstrated an average reduction in wound size

of 23 percent [15].

Debridement is another surgical method employed in wound healing, as investigated by various studies [16–19]. It involves the removal of non-viable tissue from the wound site [18]. Such tissue, often called debris or necrotic tissue, comprises substances like fibrinous, collagen, and elastin, commonly found in contaminated wounds [24]. Necrotic tissue in chronic wounds prevents keratinocyte migration to the wound bed and generates a physical barrier against wound healing [18]. Consequently, extraction of dead tissue facilitates wound healing by allowing new and healthy tissue to develop [24]. Debridement can be executed through various means, including surgical, automatic, enzymatic, biological, and mechanical methods [18]. Gauze is applied to the wound for debridement, and saline is used if moisture is required. The gauze and tissue are then surgically removed from the wound, leaving healthy tissue to promote wound closure. While effective, debridement can be uncomfortable for patients and may involve temporarily enlarging the wound to achieve its objectives. Additionally, its effectiveness may be diminished in diabetic patients [12].

Another surgical method commonly used in wound closure is mechanical closure, which includes techniques such as sutures, stapling, and wound strips. This approach is suitable for wounds that are small enough to be effectively sealed off from the external environment. By physically closing the wound, mechanical closure reduces its size and aids the healing process. However, mechanical closure is often limited by the wound size it can effectively treat. In addition, it can leave scarring, which can be a concern for some patients. Moreover, mechanical closure may not always be suitable for wounds in diabetic patients due to the unique characteristics of diabetic ulcers [12].

1.5 Non-surgical Wound Healing Methods

Surgical methods often prove inadequate for managing chronic wounds such as diabetic ulcers, pressure sores, and venous ulcers, which exhibit delayed healing. In such cases, various non-surgical approaches can be employed. Braun et al. (2013) [12] outline several non-surgical methods, including electrical stimulation, ultrasound therapy, and static magnetic field therapy. Detailed information on non-

surgical treatments is given below:

1.5.1 Wound healing with electrical stimulation

The concept of injury current, initially defined by Du Bois-Reymond in 1843, refers to the measurement of current typically around 1 mA in skin wounds [25] [29]. Subsequent studies have shown that the electric current in the wound remains below 1 mA [25]. The movement of polarized epithelial cells in both directions generates an electric field within the body. These cells have Na^+ and Cl^- channels in the outer layer and Na^+/K^+ ATPase in the inner layer. The uneven distribution of these ion channels causes an electric current within the cell, leading to the generation of trans-epidermal potentials (TEP) through directional ion transport. Research shows that when TEP is disrupted due to damage to the skin, wound currents occur [10] [26]. Studies have shown that the injury current increases by around 2 to 3 mm, while the electric field decreases from around 140 mV/mm to 0 mV/mm [25]. The wound site acts as a cathode, unlike the surrounding healthy tissue. [10]. Believed to be crucial for initiating the wound-healing process, this injury current generates a lateral electric field as it flows through the injured skin [7].

Electrical stimulation (ES) stands out as a significant alternative to traditional wound treatments, as supported by various studies [7] [10–12] [25] [27–30]. This therapeutic modality involves the application of current using electrodes either directly on the wound or close to the skin [30]. ES harnesses electrical energy to influence various physiological processes involved in wound healing, including cell proliferation, migration, and tissue regeneration. By stimulating these processes, ES promotes faster and more effective wound closure.

Three commonly used types of electrical currents in wound healing, in conjunction with electrical stimulation (ES), include direct current (DC), pulsed current (PC), and alternating current (AC) [28]. Direct current (DC) involves a continuous flow of ions in one direction for at least 1 second. The direction of current flow is determined by polarity [11]. The direct current (DC) used in electrical stimulation (ES) devices mimics the natural currents found in the body. A cathode is placed on injured tissue and an anode on healthy tissue [10]. In wound care, low-intensity direct current (LIDC) ranging from 20-1000 μA is often applied to minimize damage to

healthy tissue. LIDC is characterized by a continuous monophasic waveform with a current typically set at one mA or less [7]. Bidirectional current, which alternates polarity, aids in wound healing by organizing charged particles beneficially. Placing electrodes on healthy skin can help reduce or eliminate thermal effects, making bidirectional current less invasive and associated with fewer adverse reactions than unidirectional flow [10].

Pulsed current (PC) involves the controlled flow of electrons or ions, which can be unidirectional or bidirectional. This type of electrical stimulation is defined by its waveform parameters, such as amplitude, frequency, and duration. PC is typically administered using electrodes placed directly on the skin or wound area to target specific tissues and facilitate therapeutic effects. Pulsed current (PC) can be categorized into two primary waveforms: monophasic and biphasic. In Monophasic Pulsed Current (MPC), electrons or ions flow in one direction during each pulse and then return to the zero line after a finite period. The duration of a monophasic pulse is always less than 1 ms [11].

MPC includes various electrode configurations, such as high-voltage pulsed current (HVPC) and low-voltage pulsed current (LVPC). The treatment electrode is usually placed on the wound surface [27]. Low-voltage pulsed current (LVPC) devices utilize continuous DC, monophasic, and biphasic waveforms with longer durations and lower voltages (typically 20–35V). In contrast, high-voltage pulsed current (HVPC) involves short durations (less than 200 μs) and higher voltages ranging from 150 to 500 V. This method is specifically employed to aid in wound healing, alleviate pain, and reduce edema through electrical stimulation [7]. Bidirectional biphasic pulsed currents involve two phases of electrical flow, characterized by alternating polarity during each phase [11]. In treatments utilizing biphasic pulsed current with symmetrical waveforms, both electrodes are usually placed along the edges of the wound [27].

Transcutaneous Electrical Nerve Stimulation (TENS) is a method used to transmit a low-frequency electric current. Many studies support its effectiveness in stimulating peripheral nerves and producing physiologic effects [31–34]. Studies have indicated that low-frequency TENS increases blood volume compared to high-frequency TENS when applied at the same intensity [31] [35]. Another method used for

wound healing, particularly chronic leg ulcers, is the Frequency Rhythmic Electrical Modulation System (FREMS). This device aims to reduce the need for continuous medication and may also help to treat abnormal healing wounds and skin scars [7].

1.5.2 Wound healing method using ultrasound

Researchers have taken a new approach to wound healing using ultrasound technology. Ultrasound operates through mechanical vibrations at frequencies above the threshold of human hearing (20 kHz). Therapeutic ultrasound, typically operating at 1-3 MHz frequencies, has recently been found beneficial for wound care. Despite its long-standing use in physical therapy and sports medicine, its application in wound healing is a newer development [36–38]. On the other hand, high-frequency ultrasound (20-40 MHz) is employed as diagnostic ultrasound for anatomical analysis of the skin [38]. Ultrasound has various effects, such as thermal effects, mechanical effects, and cavitation. The creation of little bubbles and fluids inside the body is called cavitation. The ultrasound beam generates microflow with mechanical pressure waves and provides unidirectional fluid flow [37] [38].

The ultrasound transducer can produce acoustic waves with different amplitudes and frequencies. These waves can be either pulsed or continuous. Pulsed waves involve on/off cycles by adjusting the output of each transducer element. Continuous waves have a heating effect, but this thermal effect can be reduced by choosing a lower intensity [39]. Exciting piezoelectric transducers generate continuous ultrasonic waves with an external radio frequency source [40]. The pulsed waves are also used to transmit ultrasound pulses. These pulses usually operate between 0.5 and 2 milliseconds and are interspersed with pauses lasting a few milliseconds [41]. Pulsed waves are used to reduce the total energy delivered to the patient compared to continuous waves. They are preferred for wound treatment due to their non-thermal effect. Specific limits apply to the use of continuous ultrasound: low intensity $< 0.3W/cm^2$, medium intensity $0.3 - 1.2W/cm^2$, and high intensity $1.2 - 3.0W/cm^2$. Lower intensity is generally favored to achieve the desired therapeutic effect. Low-intensity ultrasound is suitable for acute injuries, while medium intensity is often used for chronic conditions. The intensity can be adjusted up to $0.5W/cm^2$ based on

temperature rise monitoring and individual circumstances. Lower-intensity pulsed waves can be applied to avoid thermal effects entirely [42].

Ultrasound possesses both physical and therapeutic effects, and if used incorrectly, it can potentially harm the body [41] [43]. These effects include thermal and non-thermal effects. Thermal effects result from the absorption of ultrasound energy, and the extent of absorption depends on the size of the area being treated. This absorption leads to an increase in cell metabolism [43] [66]. Non-thermal effects of ultrasound include cavitation and acoustic streaming [41] [43]. Ultrasound can induce the formation of micron-sized bubbles within biological tissues such as blood and lymph. These bubbles can migrate to different body parts and may burst or vibrate in response to pressure changes induced by ultrasound waves [41].

When controlling therapeutic ultrasound, it's essential to use a matching medium to minimize the effect of skin impedance. Various substances such as oils, gels, and degassed waters can effectively transmit ultrasound waves to the targeted area. A novel therapy system known as MIST (Mist Ultrasound Therapy) has been introduced for wound healing using ultrasound technology (Celleration, Inc., Eden Prairie, MN). This non-contact system utilizes a low-frequency approach to accelerate the healing process [45]. In MIST therapy, saline generates a mist that is applied to the wound area. This mist acts as a medium for transmitting ultrasound energy without directly touching the patient. The mist is sprayed onto the wound surface in vertical and horizontal directions over 4 minutes, using a 40 kHz transducer with a distal displacement of 60-70 μs [38].

In vitro studies investigating the effects of ultrasound have revealed several notable outcomes:

Collagen Production: Ultrasound treatment has been associated with increasing collagen production. This effect contributes to the growth and repair of the extracellular matrix [46].

Increased Macrophage Response: Ultrasound has been shown to enhance the response of macrophages, leading to increased cytokine production, leukocyte adhesion, and migration during the inflammatory phase [46–49].

Increased Angiogenesis: Ultrasound treatment has been linked to increased angiogenesis, the process of forming new blood vessels. This effect can aid in the delivery

of oxygen and nutrients to tissues, promoting healing [50].

Increased Nitric Oxide Production: Studies have shown that ultrasound can lead to increased nitric oxide production, which plays a role in various cellular processes, including wound healing [51].

Degranulation of Mast Cells: Ultrasound treatment has been associated with increased degranulation of mast cells, which release various bioactive molecules involved in inflammation and tissue repair [52].

Morphological Changes in Fibroblasts: Ultrasound treatment has been observed to induce morphological changes in fibroblasts, the cells responsible for synthesizing collagen and other extracellular matrix components [53].

Furthermore, the MIST ultrasound device has been the subject of experimental studies involving animals and humans. In a study using a diabetic mouse model, MIST ultrasound was found to enhance angiogenesis and collagen accumulation [54]. Another investigation conducted by Ennis et al. evaluated the efficacy of MIST ultrasound therapy (MIST Therapy; Celleration, Inc., Eden Prairie, Minn.) and revealed that after 12 weeks of treatment, artificially induced ulcers exhibited a 40.7 percent healing rate compared to 14.3 percent in the control group (p=0.0366) [67]. Additionally, in a study by Ennis et al., MIST therapy was rapid, painless, and clinically effective, with a recovery rate of 69 percent [38].

1.5.3 Wound healing using static magnetic field

Static magnetic field (SMF) therapy is a non-invasive wound healing method [55–57]. While the scientific literature on static magnetic fields is relatively limited, magnets have been utilized to hasten healing and alleviate pain, particularly within alternative medicine practices. Although comprehensive data are lacking, it is suggested that static magnetic fields may operate through three main mechanisms, as proposed in relevant literature: 1) anti-inflammatory effects, 2) promotion of endothelial cell proliferation, and 3) support for collagen formation [58].

A research study has shown that static magnetic fields (SMF) can affect the production of inflammatory cytokines [59]. Additionally, SMF has received approval from the US Food and Drug Administration (FDA) for applications in pain and edema treat-

ment by modulating cell metabolism and proliferation [60]. Prolonged exposure to SMF has been associated with the control of hypertension [61] and has shown positive effects in treating osteoarthritis and nonunion fractures [60] [62] [63]. A study in 2008 demonstrated that a 220 mT static magnetic field accelerated recovery rates in normal rats [58]. In 2016, the research explored the effects of a pulsed electromagnetic field (PEMF) with a frequency of 75 Hz and magnetic field intensity of 1 mT applied to rats using a Helmholtz coil. Simultaneously, pulsed radio frequency energy (PRFE) was applied at a carrier frequency of $27.12MHz$. This study found that rats treated with PEMF and PRFE exhibited faster wound healing compared to untreated rats [64]. Recent studies have also indicated that moderate-intensity static magnetic fields, such as 0.6 T, can improve wound healing in mouse models of type 2 diabetes resulting from genetic mutations. Additionally, lower concentrations ranging from 180-230 mT have shown beneficial effects on wound healing in mice with streptozotocin-induced diabetes [65].

1.6 Objectives of the thesis

This thesis proposes a novel non-surgical method for wound healing. It is based on the Lorentz electric field generated by ultrasonic pressure under a static magnetic field. To apply this method, an ultrasonic transducer is positioned near the wound to produce vibrations around it, which help accelerate the particles within the scar tissue. The resultant acoustic vibrations generate particle velocity. Due to static magnetic field and particle velocity, a Lorentz electric field is generated in the wound tissue. Since the wound tissue is conductive, a current density will generated in the wound. Different static magnetic fields are generated using Helmholtz coils or permanent magnets, and their impact on wound healing will be studied. Numerical simulations using the COMSOL Multiphysics program are performed to demonstrate results such as current density and pressure differences in the wound. Furthermore, animal experiments are carried out in four groups (static magnetic field group, ultrasound group, Lorentz field group, and control group) with eight rats in each group.

1.7 Thesis Outline

The numerical solutions of the Lorentz fields are detailed in Section 3. This thesis encompasses both numerical studies and animal experiments. The numerical studies utilized the finite element method-based COMSOL Multiphysics software, with the specific modules employed explained in this section. Following the explanations, the results of the numerical studies are presented in Section 3. The animal experiments were divided into four groups: 1) static magnetic field group, 2) ultrasound group, 3) Lorentz fields group, and 4) control group. Each group consisted of eight male albino Wistar rats. In the static magnetic field group, Helmholtz coils and permanent magnets were employed. The ultrasound group utilized a single-element transducer. In the proposed hybrid method, Lorentz fields were combined with a permanent magnet and a single-element transducer. Throughout the experimental period, the control group received no treatment, and the healing process of the wound was observed.

2. MATHEMATICAL BACKGROUND

This thesis presents a hybrid method that addresses multiphysics problems, requiring the simultaneous solution of electromagnetic and acoustic fields. The mathematical framework encompasses both electromagnetic and acoustic equations.

2.1 Electromagnetic Field Equations

Electromagnetic fields are computed as time-varying quantities based on Maxwell's equations: [68]

$$\nabla \times \vec{E} = -\frac{\partial \vec{B}}{\partial \vec{t}} \tag{1}$$

$$\nabla \times \vec{B} = \mu_0 \vec{J} + \mu_0 \frac{\partial \vec{D}}{\partial \vec{t}} \tag{2}$$

$$\nabla \cdot \vec{D} = \rho \tag{3}$$

$$\nabla \cdot \vec{B} = 0 \tag{4}$$

In the given equations above, $\vec{E}$ denotes the electric field, $\vec{B}$ the static magnetic field, $\vec{J}$ the current density, and $\vec{D}$ the displacement. Additionally, $\vec{\mu_0}$ refers to the free permeability.

To solve the above equations we need the continuity condition:

$$\nabla \cdot \vec{J} = -\frac{\partial \rho}{\partial t} \tag{5}$$

And the constitutive relations:

$$\vec{D} = \epsilon \vec{E} \tag{6}$$

$$\vec{J} = \sigma \vec{E} + \sigma(\vec{v} \times \vec{B}) \tag{7}$$

the expression $\vec{v} \times \vec{B}$ represents the Lorentz field where $\vec{v}$ is the velocity of the conductor and $\vec{B}$ is the magnetic flux density. The second term of the Equation 7 is

called velocity current density. Given $\vec{B}$ is zero (as Equation 4), and magnetic vector potential $\vec{A}$ as:

$$\vec{B} = \nabla \times \vec{A} \tag{8}$$

As a result, $\vec{E}$ can be denoted as the electric field, the magnetic vector potential $\vec{A}$ and the scalar potential φ gradient as:

$$\vec{E} = -\nabla\varphi - \frac{\partial \vec{A}}{\partial t} \tag{9}$$

For the proposed 2D wound model, we assume a thickness in the xy plane. The electric field $\vec{E}$ and particle velocity $\vec{v}$ refer to the xy directions, while the magnetic flux density B refers only to the z component. Equation (1) in a more streamlined and computationally efficient manner, considering the context of Lorentz fields for wound healing:

$$\nabla \times \vec{E} + \frac{\partial \vec{B}}{\partial t} = 0 \tag{10}$$

The electric field $\vec{E}$ components given by Equation 7:

$$\vec{E} = \frac{\vec{J}}{\sigma} - \vec{v} \times \vec{B} \tag{11}$$

It is rewritten according to Equation 2,

$$\vec{E} = \frac{\nabla \times \vec{B}}{\mu_0 \sigma} - \vec{v} \times \vec{B} \tag{12}$$

Therefore, Equation 10) is written as follows [69]:

$$\frac{1}{\mu_0}\nabla \times (\frac{1}{\sigma}\nabla \times \vec{B} - \vec{v} \times \vec{B}) + \frac{\partial \vec{B}}{\partial t} = 0 \tag{13}$$

2.2 Basic Acoustic Field Equations

To simplify our analysis, let us assume a source-free and lossless environment. Initially, we consider a one-dimensional (1D) scenario. In the static case, the pressure within the body remains constant and is represented by p_0. The body's mass den-

sity $\rho_0(x)$ is considered to be position-dependent. In the presence of a propagating pressure wave, the total pressure p_T varies with both position and time, and it is expressed as:

$$p_T(x,t) = p_0 + p(x,t) \tag{14}$$

In such a scenario, the total mass density:

$$p_T(x,t) = \rho_0 + p(x,t) \tag{15}$$

Ultrasound waves cause small displacements of elements within the body, leading to a corresponding 'particle velocity', $v(x,t)$. And the 'equation of motion' as:

$$-\partial p/\partial x = \rho_0 \partial v/\partial t \tag{16}$$

particles accelerate against the pressure gradient. This phenomenon is described by the continuity equation, which is written as:

$$-\frac{\partial \rho_T}{\partial t} = \frac{\partial(\rho_T v)}{\partial x} \tag{17}$$

which simplifies to the following after linearization (under the above-mentioned conditions):

$$-\frac{\partial \rho}{\partial t} = \rho_0 \frac{\partial v}{\partial x} \tag{18}$$

To derive a differential equation relating p and ρ, we need to eliminate the particle velocity term in Equations (16) and (18). This can be accomplished by employing a constitutive equation that relates them. If the change in mass density ρ depends only on changes in pressure p, then a linearized constitutive equation can be written as:

$$\rho = [\partial \rho/\partial p]_{p=0}/p = \rho_0 \beta_0 p \tag{19}$$

where β_0 is the compressibility defined as

$$\beta_0 = -\frac{1}{V}\frac{\partial V}{\partial p} \tag{20}$$

Following is the derivation Equations (16), (18), and (19). Taking the spatial derivative of Equation (16) we obtain,

$$-\frac{\partial^2 p}{\partial x^2} = -\frac{\partial^2 \rho}{\partial t^2} + (-\frac{1}{\rho_0}\frac{\partial p}{\partial x})\frac{\partial \rho_0}{\partial x} \tag{21}$$

Using the linearized constitutive Equation (19) we obtain

$$\frac{1}{c_s^2}\frac{\partial^2 p}{\partial t^2} = \frac{\partial^2 p}{\partial x^2} - \frac{\partial p}{\partial x}(\frac{1}{\rho_0}\frac{\partial \rho_0}{\partial x}) \tag{22}$$

Where $c_s^2 = (\rho_0 \beta_0)^{-1}$ represents the speed at which pressure waves propagate. Multiplying both sides by $1/\rho_0$, and upon rearranging the terms on the right-hand side of the equation, we obtain:

$$\frac{1}{\rho_0 c_s^2}\frac{\partial^2 p}{\partial t^2} = \frac{\partial}{\partial x}(\frac{1}{\rho_0}\frac{\partial p}{\partial x}) \tag{23}$$

The equation of motion (Equation (16)) used in the previous derivation remains applicable, considering the presence of additional force terms. We can disregard gravitational force terms. When magnetic flux density $\vec{B}$ and charged particles (current density $\vec{J}$) are present in the body, the equation of motion is modified to include the Lorentz force per unit volume $\vec{q} = \vec{J} \times \vec{B}$ in addition to the mechanical forces within the body. Therefore, the modified equation of motion is:

$$q_x - \partial p/\partial x = \rho_0 \, \partial v/\partial t \tag{24}$$

Where q_x denotes the x-component of this interaction. Considering the movement of charged particles and their resulting current density $\vec{J} = \sigma\vec{E} + \sigma(\vec{v} \times \vec{B})$ the wave equation should be modified to incorporate the effects of Lorentz forces. This yields:

$$\frac{1}{\rho_0 c_s^2}\frac{\partial^2 p}{\partial t^2} = \nabla \cdot [\frac{1}{\rho_0}(\nabla p - \vec{q})] \tag{25}$$

In this study, the pressure distribution within the medium, assumed to be source-free, is solely influenced by the boundary conditions imposed by an ultrasonic transducer in contact with the medium. The specific boundary conditions are as follows:

$$\frac{1}{\rho_0}(\nabla p - \vec{q}) \cdot \vec{n} = \ a_n \ on \ S_T \tag{26}$$

At the interface S_T where the body surface contacts the transducer, the boundary condition ensures the continuity of acceleration. The term a_n in Equation (26) represents the local acceleration caused by the transducer at the interface S_T. This term is derived from the mechanical interaction between the transducer and the medium, as discussed in the next section of the study:

$$\frac{\partial \vec{v_1}}{\partial t} \cdot \vec{n} = \frac{\partial \vec{v_2}}{\partial t} \cdot \vec{n} \tag{27}$$

This equation $\vec{v_1}$ and $\vec{v_2}$ represents the continuity of normal particle velocity components across an interface between two regions or media. Where $\vec{v_1}$ and $\vec{v_2}$ denote the particle velocities in region 1 and region 2 of an interface, respectively [69]:

$$\frac{1}{\rho_{01}}(\nabla p - \vec{q})_1 \cdot \vec{n} = \frac{1}{\rho_{02}}(\nabla p - \vec{q})_2 \cdot \vec{n} \qquad\qquad on \ S \tag{28}$$

3. NUMERICAL MODELING

The proposed method for enhancing wound healing involves the generation of Lorentz fields, achieved by applying ultrasound within a static magnetic field environment. The ”Mathematical Background” delves into the formulations concerning pressure acoustics and scalar and magnetic vector potentials. This section elaborates on the numerical modeling techniques employed to simulate the proposed healing method.

To solve the problem numerically, the software COMSOL Multiphysics is used. This software package is designed to analyze and simulate diverse physics and engineering problems. It utilizes advanced finite element analysis techniques to handle complex multiphysics phenomena and solve partial differential equations [70]. In our problem, the acoustic, piezoelectric, and electromagnetic modules are solved simultaneously. Specific physics properties with coupling parameters characterize each module.

3.1 Model Geometry

A 2D model geometry is constructed to solve the coupled problem numerically (Figure 3.2 and Figure 3.3). For the 2D model generated, two separate ultrasonic transducers were used. The first method used a 16-element LPA transducer and the second used a single-element ultrasonic transducer. The wound characteristics and dimensions used in both methods are the same. The geometry comprises the ultrasonic transducer, skin, wound, and the surrounding air. The layers of the skin, epidermis, dermis, hypodermis, and wound were defined in this model. The thickness of the epidermis was 1 mm [77–79], the thickness of the dermis was 2 mm [80–83], the thickness of the hypodermis was 10 mm [84] and the depth of the wound was 7 mm [85]. The width of the wound was 20 mm and the width of the healthy skin around the wound was 5 mm.

3.2 Ultrasonic Transducer

In our simulations, we modeled two types of ultrasonic transducers: a 16-element linear phased array transducer and a single-element transducer. Specifically, we used

PZT-5H material to model the ultrasonic transducer. In this study, the resonance frequency of the piezoelectric element is considered as 1MHz. The two-dimensional model of a single-element transducer has 1 mm thickness and 1 cm length (Figure 3.3). The following values were used for the dimensions of the 16-element Linear Phased Array (LPA) Ultrasonic Transducer used in the model (Figure 3.1).

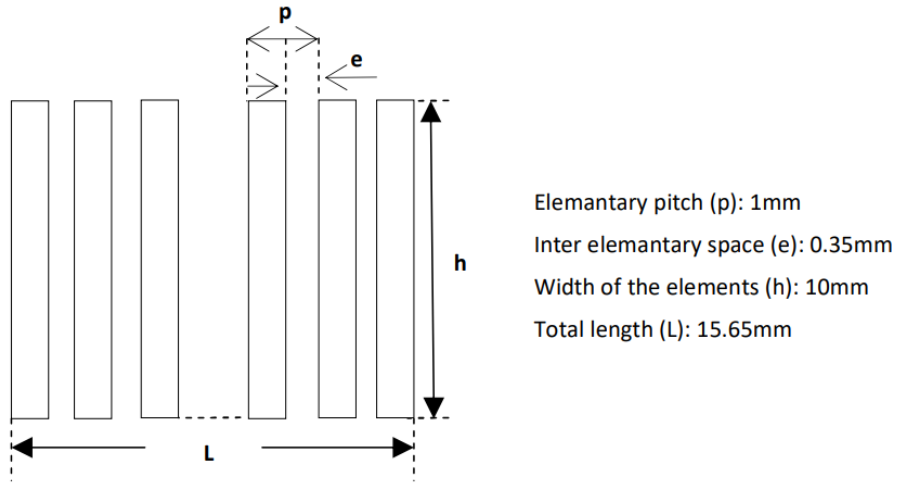


Figure 3.1 : Specifications of the 16-Element LPA Ultrasonic Transducer. [86]

3.3 Skin and Wound Modeling

Healthy skin and wound are modeled as 30mmx13mm and 20mmx13mm in size, respectively. The skin's and wound's electrical and acoustic properties are represented by the epidermis, dermis, hypodermis, blood (in the wound), and ultrasonic gel. The electrical conductivities at 1 MHz are as follows: epidermis: 0.018 S/m, dermis: 0.434 S/m, hypodermis: 0.009 S/m, blood: 0.822 S/m, and ultrasonic gel: 0.1 S/m [72–75].

To solve acoustic problems effectively, it is necessary to define the acoustic properties of various body tissues and materials. The acoustic properties of skin and wound are defined as density of epidermis 1200 kg/m^3, speed of sound in it is 1645 m/s; dermis 1200 kg/m^3, speed of sound in it is 1595 m/s; hypodermis 1109 kg/m^3, speed of sound in it is 1624 m/s; blood 1040 kg/m^3, speed of sound in it is 1580 m/s and ultrasonic gel 983 kg/m^3, speed of sound in it is 1516 m/s.

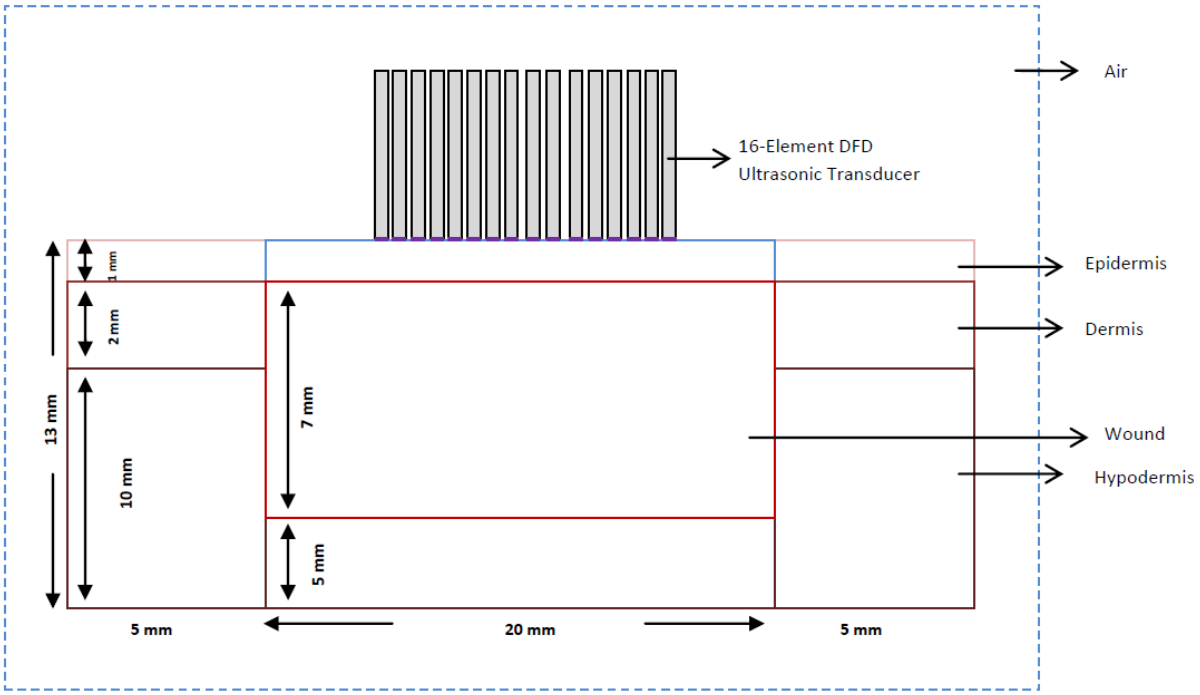


Figure 3.2 : LPA Wound Model in Comsol Multiphysics. The model defines the ultrasonic transducer, air, wound, skin layers, and skin dimensions.

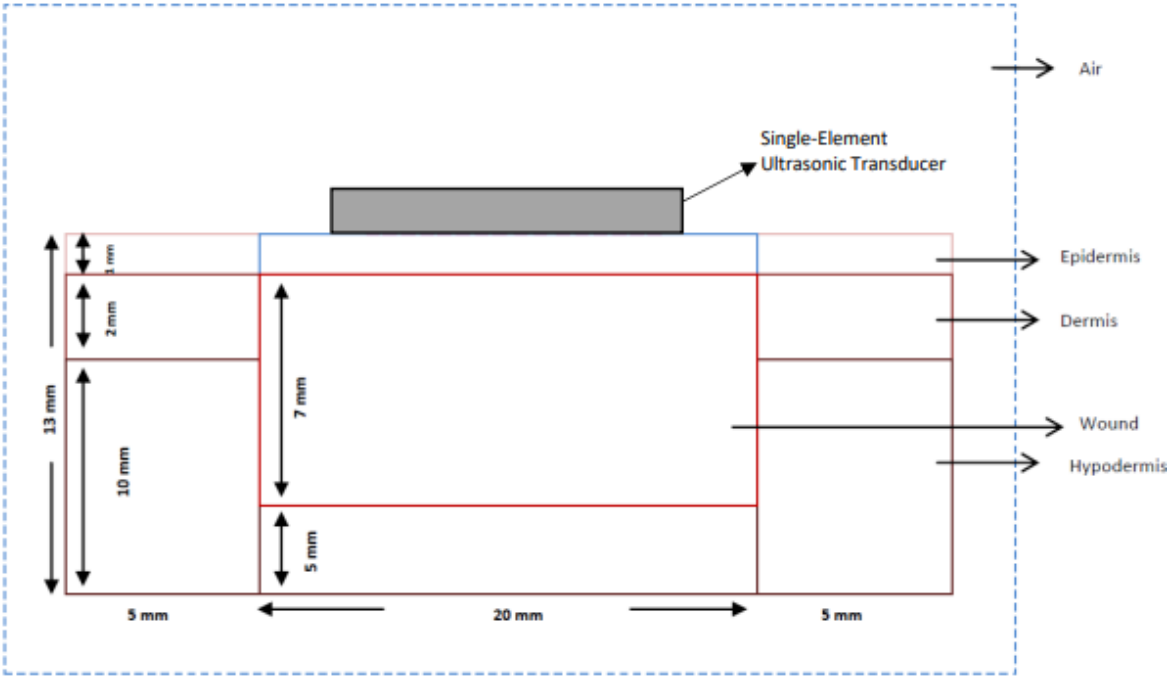


Figure 3.3 Single Element Wound Model in Comsol Multiphysics. The model defines the ultrasonic transducer, air, wound, skin layers, and skin dimensions.

Tissue	Electrical Cond. (S/m)	Density (kg/m^3)	Speed of Sound (m/s)
Epidermis	0.018	1200	1645
Dermis	0.434	1200	1595
Hypodermis	0.009	1109	1624
Blood	0.822	1040	1580
Ultrasonic Gel	0.1	983	1516

Table 3.1 : Parameters used in the model, including electrical conductivity (at 1 MHz frequency), density, and speed of sound for different tissue types [72–75].

3.4 Pressure Acoustic Module

This module addresses issues in acoustics, acoustic-structure interactions, pressure, vibrations, acoustic fields, and other acoustics-related areas. The physics interfaces used are fully multiphysics-enabled, making them easily compatible with any interface used in COMSOL Multiphysics [76]. The Pressure Acoustics Module, located within the Acoustic Module category, analyzes the acoustic properties within each subdomain and evaluates boundary conditions. Figure 3.2 shows the geometry of the model and Figure 3.4 shows the geometry with subdomains. There are seven subdomains, namely, ultrasonic gel (Ω_1), epidermis (Ω_2), dermis (Ω_3), hypodermis (Ω_4), wound (Ω_5), ultrasonic transducer (Ω_6), and surrounding air (Ω_7) in this model.

The boundaries of each domain are represented by ($\partial\Omega_1$), ($\partial\Omega_2$), ($\partial\Omega_3$), ($\partial\Omega_4$), ($\partial\Omega_5$), ($\partial\Omega_6$) and ($\partial\Omega_7$) respectively.

Equation (22) presents the general formulation for sound waves in a lossless medium, expressed in terms of acoustic pressure, *p*. In COMSOL, it is represented as follows:

$$\frac{1}{\rho_0 c_s^2}\frac{\partial^2 p}{\partial t^2} + \nabla \cdot [-\frac{1}{\rho_0}(\nabla p - \vec{q})] = Q \tag{29}$$

In this context, $\rho\ (kg/m^2)$ represents the density of the medium, $c_s\ (m/s)$ denotes the speed of sound, $\vec{q}\ (N/m^3)$indicates dipole sources (optional), and $Q(1/s^2)$ denotes monopole sources (optional). There are no monopole sources for our specific case, making the right-hand side of Equation (29) zero. However, mechanical forces such as those induced by gravity and vibrations from Lorentz fields exist and can

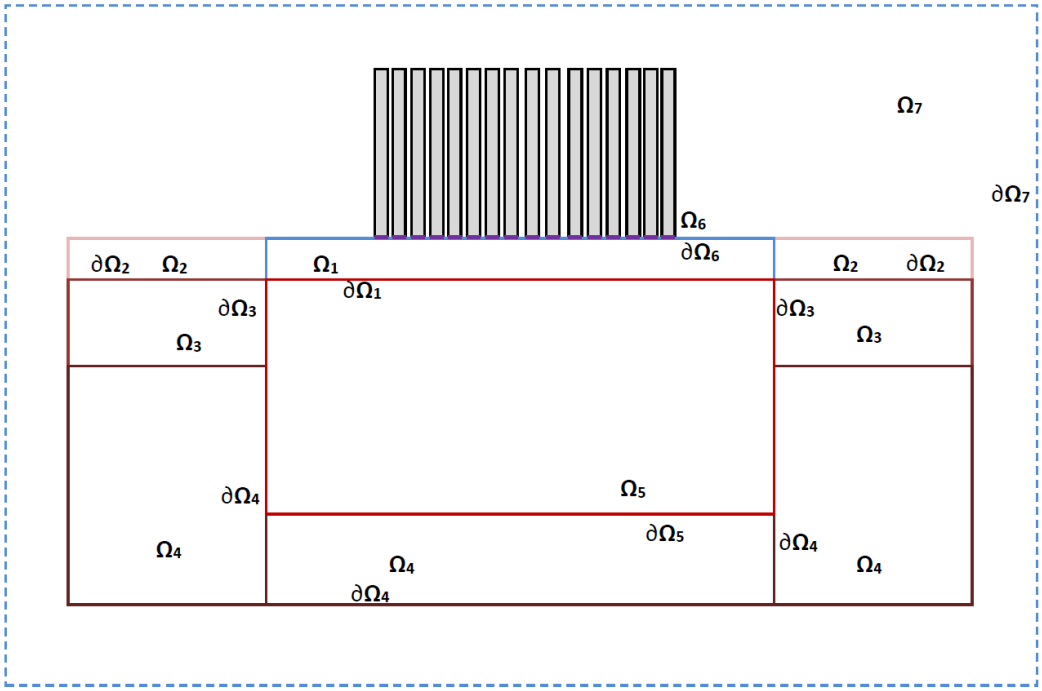


Figure 3.4 : Geometry of the pressure acoustic problem. Subdomains Ω_1, Ω_2, Ω_3, Ω_4, Ω_5, Ω_6, Ω_7 and associated boundaries $\partial\Omega_1$, $\partial\Omega_2$, $\partial\Omega_3$, $\partial\Omega_4$, $\partial\Omega_5$, $\partial\Omega_6$ and $\partial\Omega_7$ represent the ultrasonic gel, epidermis, dermis, hypodermis, wound, ultrasonic transducer and air, respectively.

be represented as dipole sources. This study assumes the body to be stationary in space under the influence of external forces, with the gravitational force effect being disregarded. The formulation must account for the non-zero Lorentz force per unit volume $\vec{q} = \vec{J} \times \vec{B}$, where $\vec{J}$ is the current density and $\vec{B}$ is the magnetic flux density present in the medium.

Boundary Conditions: Seven distinct boundaries are visually represented in Figure 3.4. Here is a summary of the properties associated with each boundary:

On $\partial\Omega_1, \partial\Omega_2, \partial\Omega_3, \partial\Omega_4$ and $\partial\Omega_5$: These boundaries maintain the continuity of the normal acceleration. The resulting equation is written as follows:

$$\vec{n} \cdot (\frac{1}{\rho}(\nabla p - \vec{q}))_1 - \vec{n} \cdot (\frac{1}{\rho}(\nabla p - \vec{q}))_2 = 0 \tag{30}$$

or

$$\vec{n} \cdot (\frac{1}{\rho}(\nabla p - \vec{q}))_1 = \vec{n} \cdot (\frac{1}{\rho}(\nabla p - \vec{q}))_2 \tag{31}$$

On $\partial\Omega_6$: This boundary refers to the interface between the ultrasonic gel and the ultrasonic transducer. Ultrasonic pressure is generated at the interface where the acoustic pressure module and the piezoelectric module are coupled. When a specific voltage excites the ultrasonic transducer at this boundary, it causes displacement in the x, y, and z directions. The acceleration component normal to the propagation direction is defined as follows:

$$\vec{n} \cdot (\frac{1}{\rho}(\nabla p - \vec{q})) = \ a_n \tag{32}$$

where a_n denotes the inward acceleration. This is obtained as the second-time derivative of the displacement at the lower boundary of the crystal in the piezoelectric problem.

On $\partial\Omega_7$: With this boundary condition, reflections at the boundary are disregarded:

$$\vec{n} \cdot (\frac{1}{\rho}(\nabla p - \vec{q})) + \frac{1}{c\rho}\frac{\partial p}{\partial t} = \frac{(1 - (\overrightarrow{n_k} \cdot \vec{n}))}{c\rho} \cdot \frac{\partial p_0}{\partial t} \tag{33}$$

Here, p_0 denotes the pressure source, q_0 represents a dipole source, and$\vec{n_k}$ denotes the wave direction. Assuming the body is lossless, the second term on the left-hand side of Equation (33) is zero. Moreover, with no external pressure sources, Equation (33) simplifies to [69]:

$$\vec{n} \cdot (\frac{1}{\rho}(\nabla p - \vec{q})) = 0 \tag{34}$$

3.5 Piezoelectric Module

The piezoelectric effect describes converting electrical energy into mechanical energy and vice versa. The direct piezoelectric effect occurs when a piezoelectric crystal undergoes deformation, leading to the polarization of electric charges in a fixed direction. This polarization is directly proportional to the deformation applied

to the crystal and generates an electric potential difference across its surfaces [71]. Applying a potential difference to the piezoelectric crystal causes deformation, resulting in pressure exerted on the body. The potential difference applied to the piezoelectric crystal generates pressure in the body. We refer to the model in Figure 3.5 to describe the piezoelectric properties and determine the boundary properties. According to this model, it is considered that only region Ω_6 exhibits piezoelectric properties.

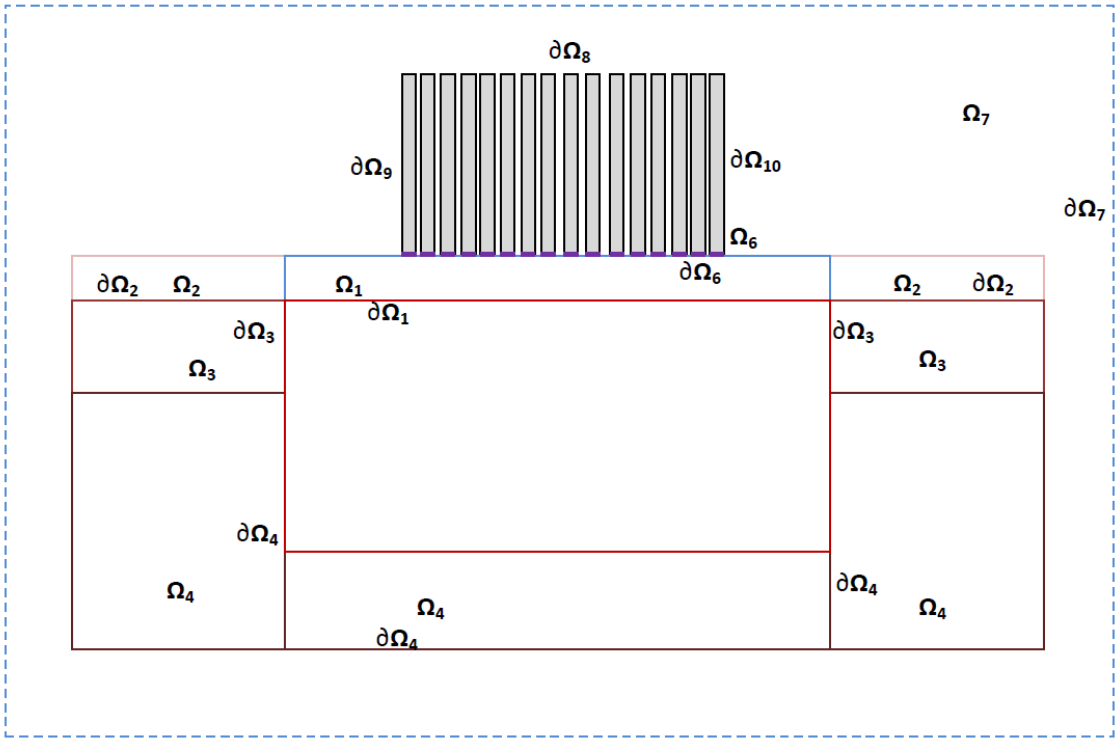


Figure 3.5 : p Geometry for the piezoelectric module. Subdomains Ω_1, Ω_2, Ω_3, Ω_4, Ω_6, Ω_7 and associated boundaries $\partial\Omega_1$, $\partial\Omega_2$, $\partial\Omega_3$, $\partial\Omega_4$, $\partial\Omega_6$ and $\partial\Omega_7$ represent the ultrasonic gel, epidermis, dermis, hypodermis, ultrasonic transducer and air, respectively. $\partial\Omega_6$ represents the surface of the crystal where the voltage is applied. On $\partial\Omega_9$ and $\partial\Omega_10$ the assumption is made that the normal component of the electrical displacement is zero. The boundary $\partial\Omega_8$ acts as the electrical ground in the problem.

Electrical Boundary Conditions:

$\partial\Omega_6$: (**Electric Potential**) The applied voltage is defined by this boundary condition. It specifies the value of the electric potential at this boundary condition.

$\partial\Omega_8$: (**Ground**) This boundary condition indicates that the surface functions as the electrical ground.

$\partial\Omega_9$ **and** $\partial\Omega_{10}$: **(Zero Charge/Symmetry)** Within these limits, the condition that

the standard component $\vec{D}$ of the electrical displacement is zero is maintained and expressed as $\vec{n} \cdot \vec{D} = 0$. The boundary $\partial\Omega_7$ does not form a direct interface. Since the body does not have piezoelectric properties. The body itself does not possess piezoelectric properties, and this boundary remains passive.

Mechanical Boundary Conditions:

$\partial\Omega_6$**,** $\partial\Omega_9$ **and** $\partial\Omega_{10}$: **(Free)** This boundary condition applies to all boundaries managed by the piezoelectric interface.

$\partial\Omega_8$: **(Roller)** It contrasts with the standard mechanical condition (free). This boundary condition that allows tangential displacements also indicates no perpendicular displacement.

3.6 Electromagnetic Module

The analysis in this module involves solving Maxwell's equations. Initially, there is only a static magnetic field. When this static magnetic field combines with an acoustic signal, it generates a Lorentz electric field and current density in the tissue. The geometrical model of this problem is illustrated in Figure 3.6.

This module's quasistatic analysis assumes that $\frac{\partial \vec{D}}{\partial t} = 0$, indicating negligible displacement currents. Detailed partial differential equations are given in Chapter 2. These equations are implemented and simulated using the AC-DC Module in COMSOL, specifically focusing on quasi-static conditions, plane induction, and magnetic fields:

$$\frac{\partial \mu_0 \mu_r \vec{H}}{\partial t} + \frac{\partial \vec{B_r}}{\partial t} + \nabla \times (\sigma^{-1}(\nabla \times \vec{H} - \vec{J^e}) - \vec{v} \times (\mu_0 \mu_r \vec{H} + \vec{B_r})) = 0 \tag{35}$$

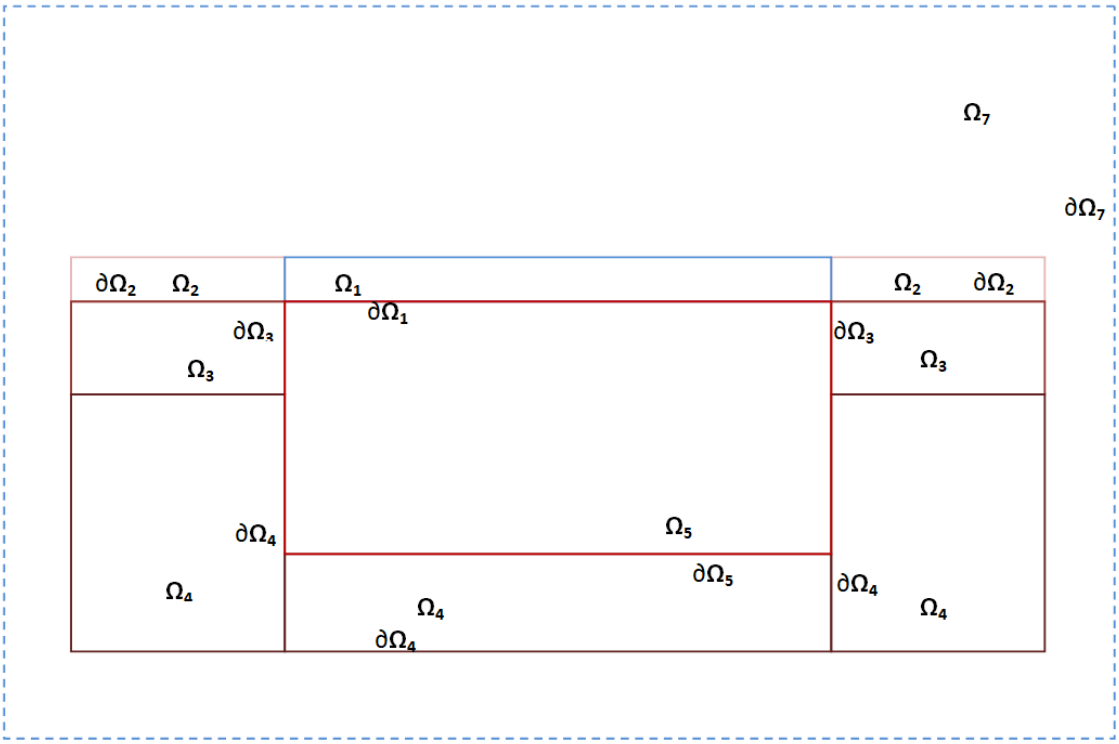


Figure 3.6 : Geometry of the electromagnetic problem. Subdomains Ω_1, Ω_2, Ω_3, Ω_4, Ω_5, Ω_7 and associated boundaries $\partial\Omega_1$, $\partial\Omega_2$, $\partial\Omega_3$, $\partial\Omega_4$, $\partial\Omega_5$ and $\partial\Omega_7$ represent the ultrasonic gel, epidermis, dermis, hypodermis and air, respectively.

$\vec{J^e}$ represents the external current density, and B_r represents the remanent flux density. This refers to the magnetic flux density remaining in a substance. There is a static magnetic flux density in the z direction of 1 Tesla. Equation (37) can, therefore, be written as follows:

$$\frac{\partial \mu_0 \mu_r \vec{H}}{\partial t} + \nabla \times (\sigma^{-1}(\nabla \times \vec{H}) - \vec{v} \times (\mu_0 \mu_r \vec{H})) = 0 \tag{36}$$

To solve Equation (38), the following boundary conditions are defined:

$\boldsymbol{\partial\Omega_1, \partial\Omega_2, \partial\Omega_3, \partial\Omega_4}$ **:** At this boundary, the continuity condition applies, ensuring that the tangential component of the electric field remains continuous across the boundary:

$$\vec{n} \times (\vec{E_1} - \vec{E_2}) = 0 \tag{37}$$

$\partial\Omega_5$: The same boundary condition (Equation 39) is defined on $\partial\Omega_1, \partial\Omega_2, \partial\Omega_3, \partial\Omega_4$.
$\partial\Omega_7$: On this boundary, the magnetic insulation condition holds, which dictates that the tangential component of the electric field is zero [69]:

$$\vec{n} \times \vec{E} = 0 \tag{38}$$

3.7 Numerical Studies Results

To find solutions using Lorentz fields, numerical methods such as the Finite Element Method (FEM) are employed. This research used the COMSOL Multiphysics program to obtain numerical solutions. This section presents the findings obtained from various simulation studies. A 16-element LPA ultrasonic transducer and a Single-element transducer were used in the numerical analysis. The 16-element transducer was positioned at different angles to visualize the wound's pressure and velocity flow density values; the results obtained are presented in Table 3.2. Additionally, results were obtained by focusing ultrasonic pressure. For focused ultrasound, the crystals in the transducer were configured in two, four, and six arrangements, and the results obtained are presented in Table 3.3. The results obtained with the single-element transducer are given in Section 3.7.2.

3.7.1 Transducer excitation

In this study, a sinusoidal voltage V is applied to the surface of a piezoelectric crystal for one period of the excitation frequency *f*, i.e.,

$$V(t) = Asin(2\pi ft) \qquad (t < 1/f) \tag{39}$$

where the amplitude term A =100V. The corresponding voltage waveform is given in. The depth of the conductive body is assumed 1.3 cm. Since the speed of sound in the body is 1520 m/s, to obtain information about the body data should be taken in duration calculated as:

$$x = vt \rightarrow t = \frac{x}{v} = \frac{1,3cm}{1520m/s} \cong 8,55\mu s \tag{40}$$

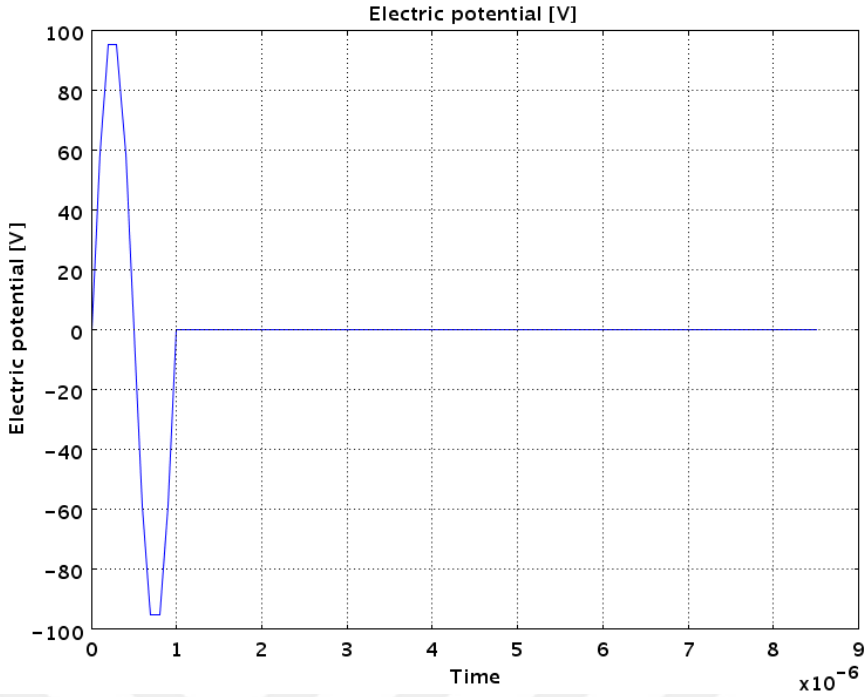


Figure 3.7 Applied voltage (V) to each piezoelectric crystal. The amplitude of the electrical signal is selected as 1 V as given in the y-axis. The x-axis shows time in seconds [69].

In this study, the run-time for each simulation is chosen as 8.55 μs with 0.1 μs intervals.

3.7.2 Single Element model results

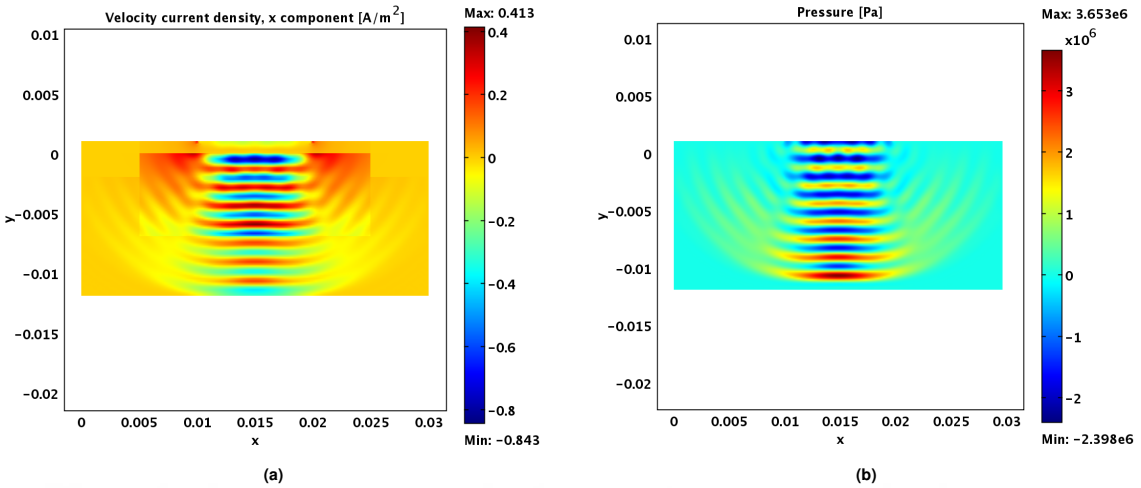


Figure 3.8 a) Current density and **b)** pressure distribution in the wound area for a Single-Element transducer driven with a 100 V signal (t = 8 μs).

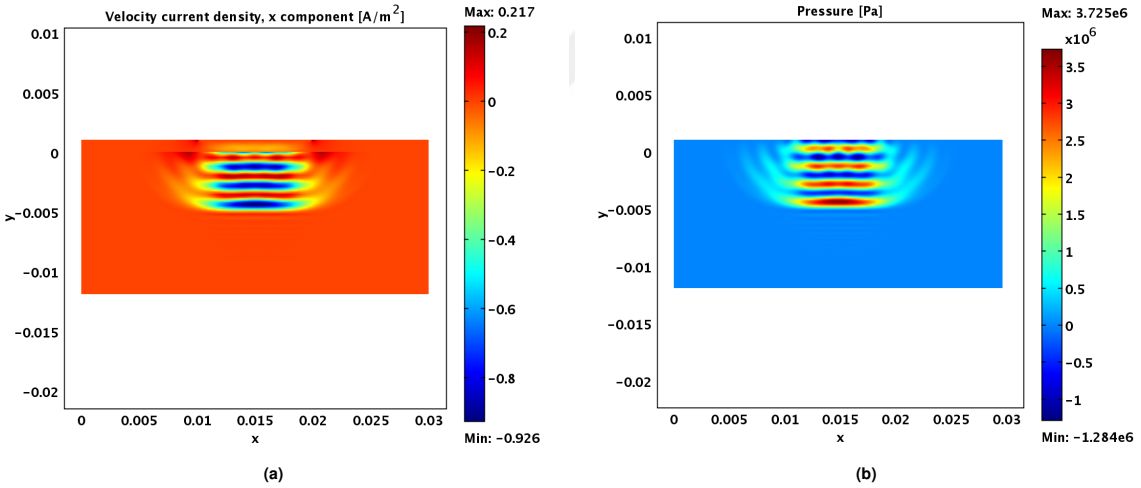


Figure 3.9 a) Current density and **b)** pressure distribution in the middle of the wound area for a Single-Element transducer driven with a 100 V signal (t = 4 μs).

3.7.3 Results from different steering angles

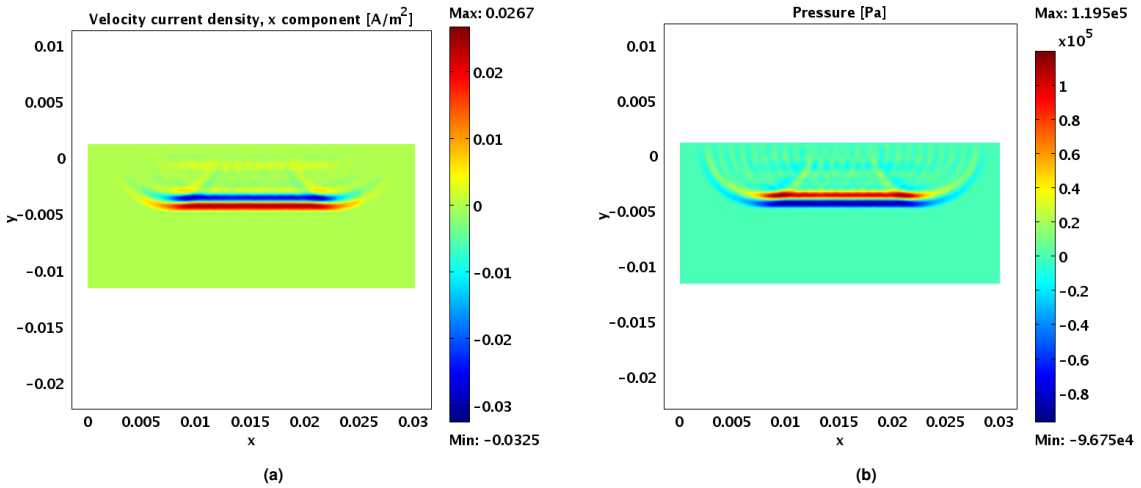


Figure 3.10 a) Current density and **b)** pressure distribution in the middle of the wound area for a 16-element LPA transducer driven with a 100 V signal (t = 4 μs).

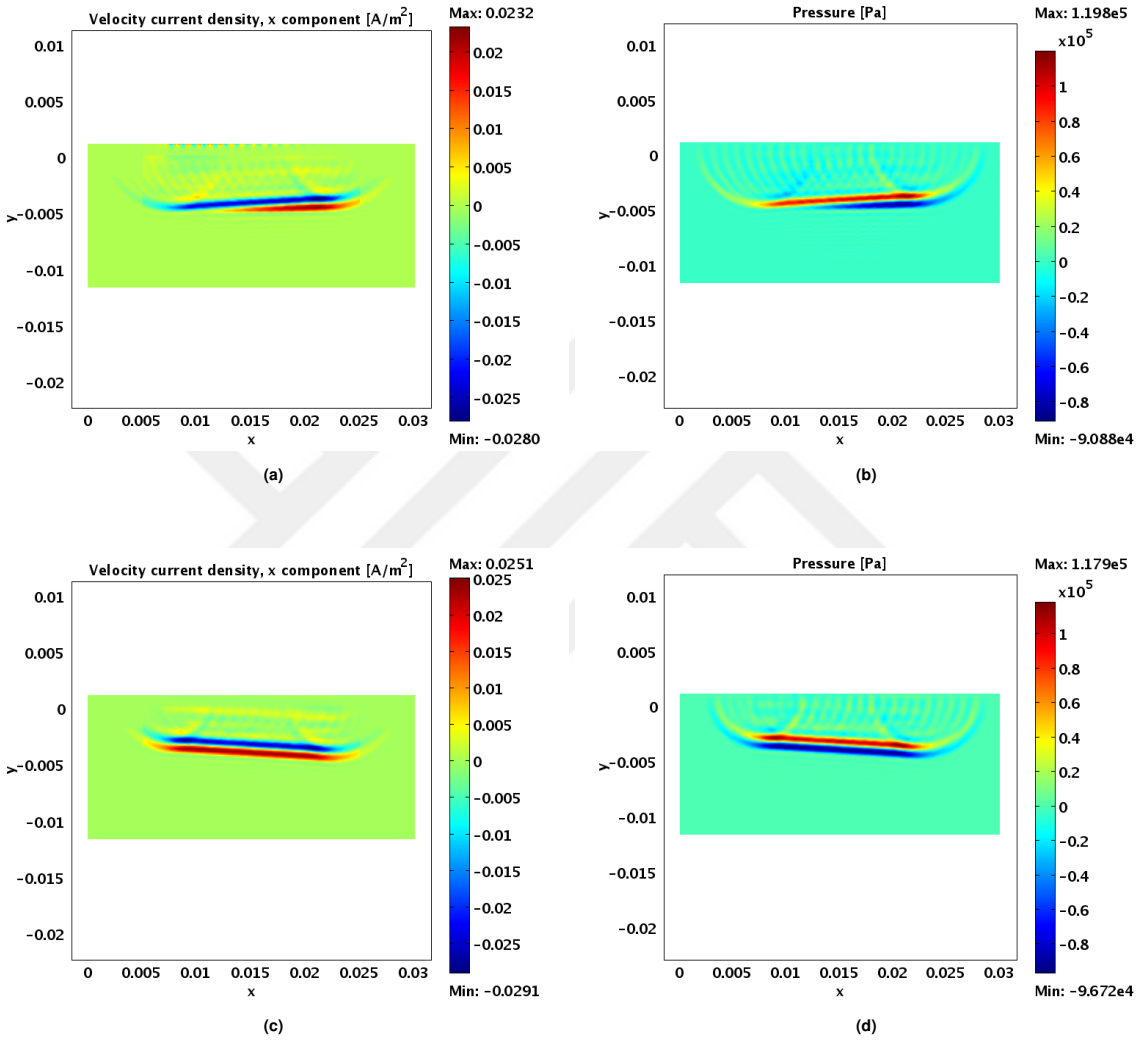


Figure 3.11 Current density (**a, c**) and pressure (**b, d**) distributions in the middle of the wound area for a 16-element LPA transducer driven with 100 V and a full signal (t = 4 μs) at -5 degree (**a, b**) and $+5$ degree (**c, d**) orientations.

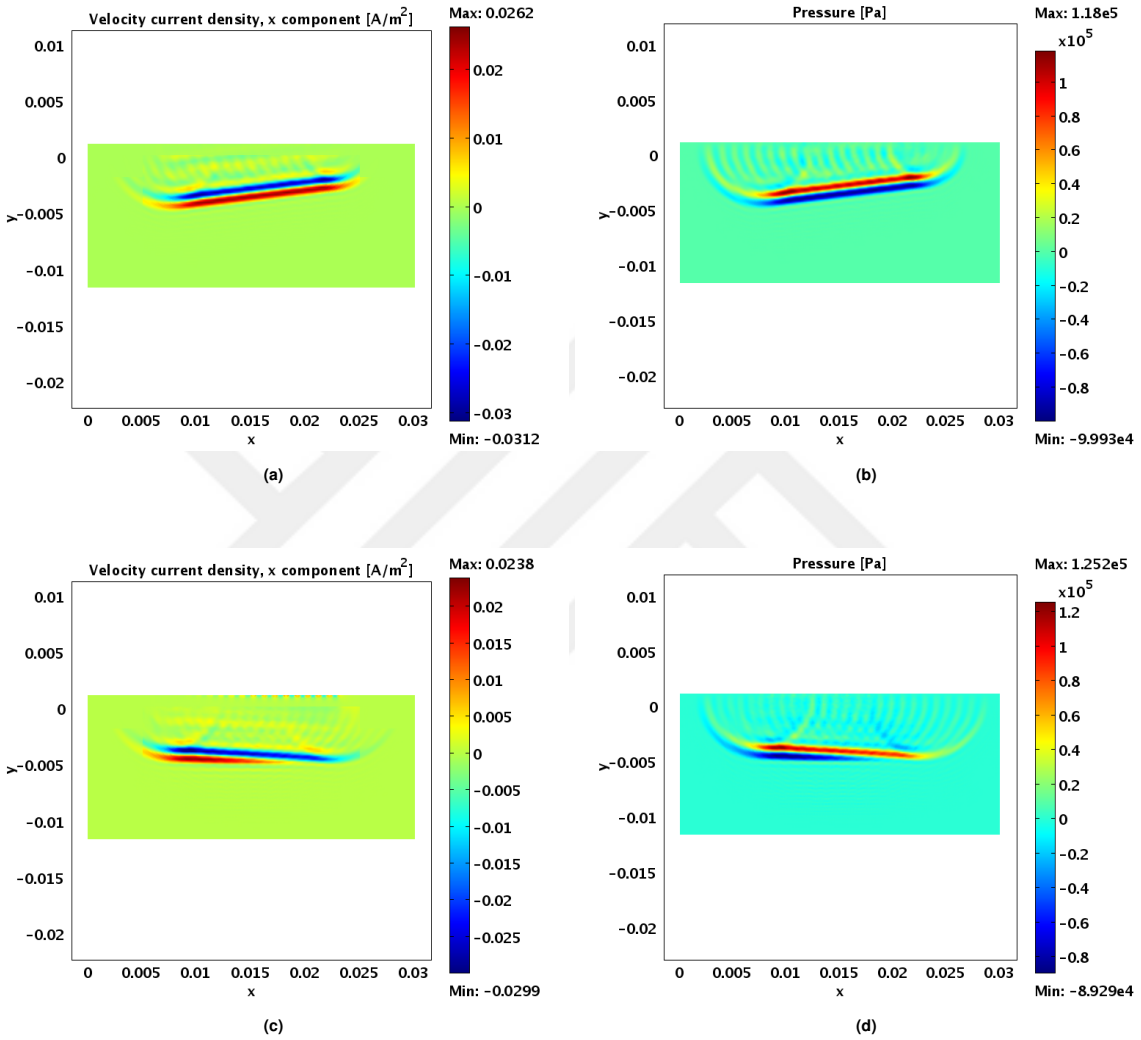


Figure 3.12 Current density (**a, c**) and pressure (**b, d**) distributions in the middle of the wound area for a 16-element LPA transducer driven with 100 V and a full signal (t = 4 μs) at -10 degree (**a, b**) and $+10$ degree (**c, d**) orientations.

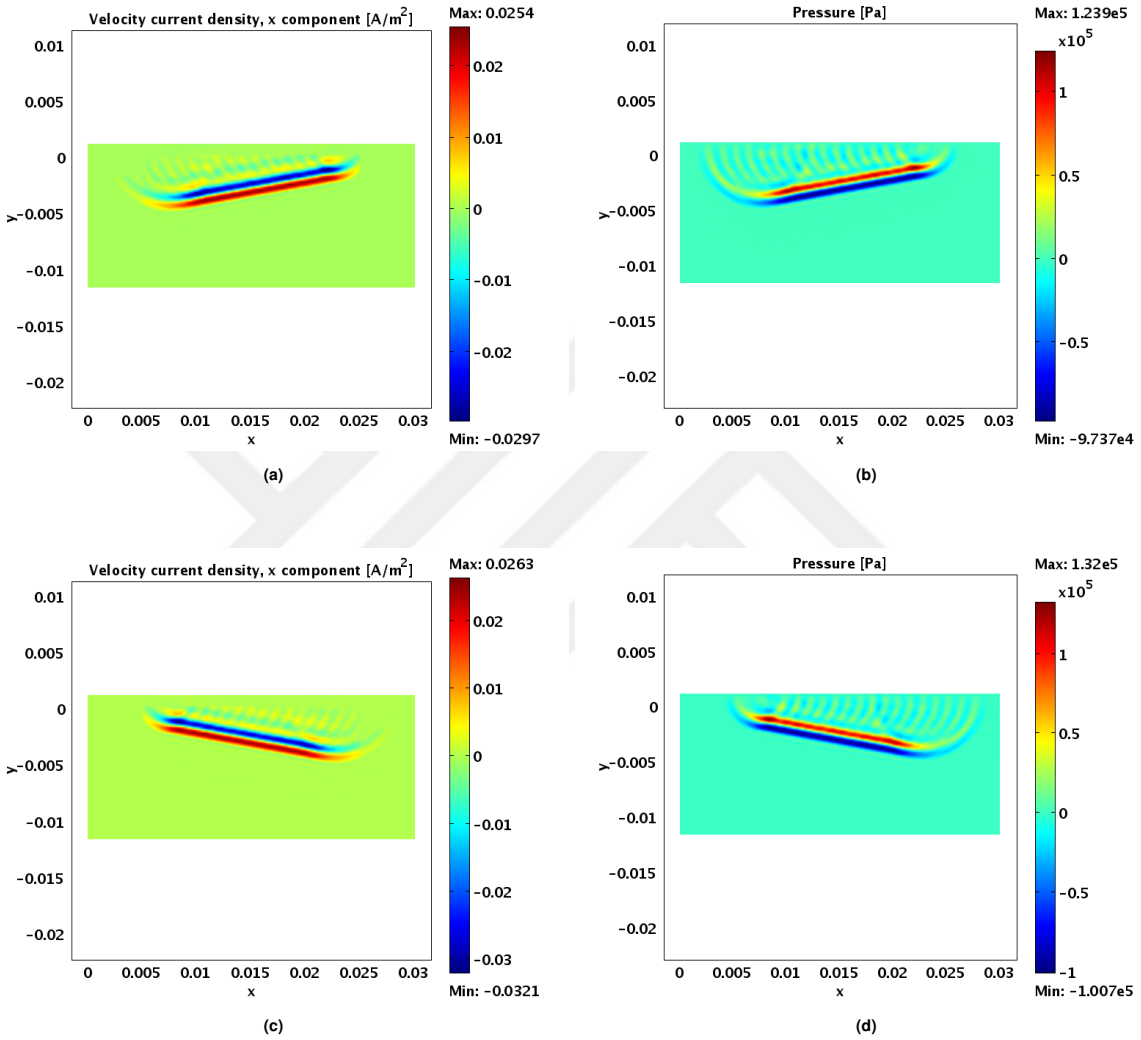


Figure 3.13 Current density (**a, c**) and pressure (**b, d**) distributions in the middle of the wound area for a 16-element LPA transducer driven with 100 V and a full signal (t = 4 μs) at -15 degree (**a, b**) and $+15$ degree (**c, d**) orientations.

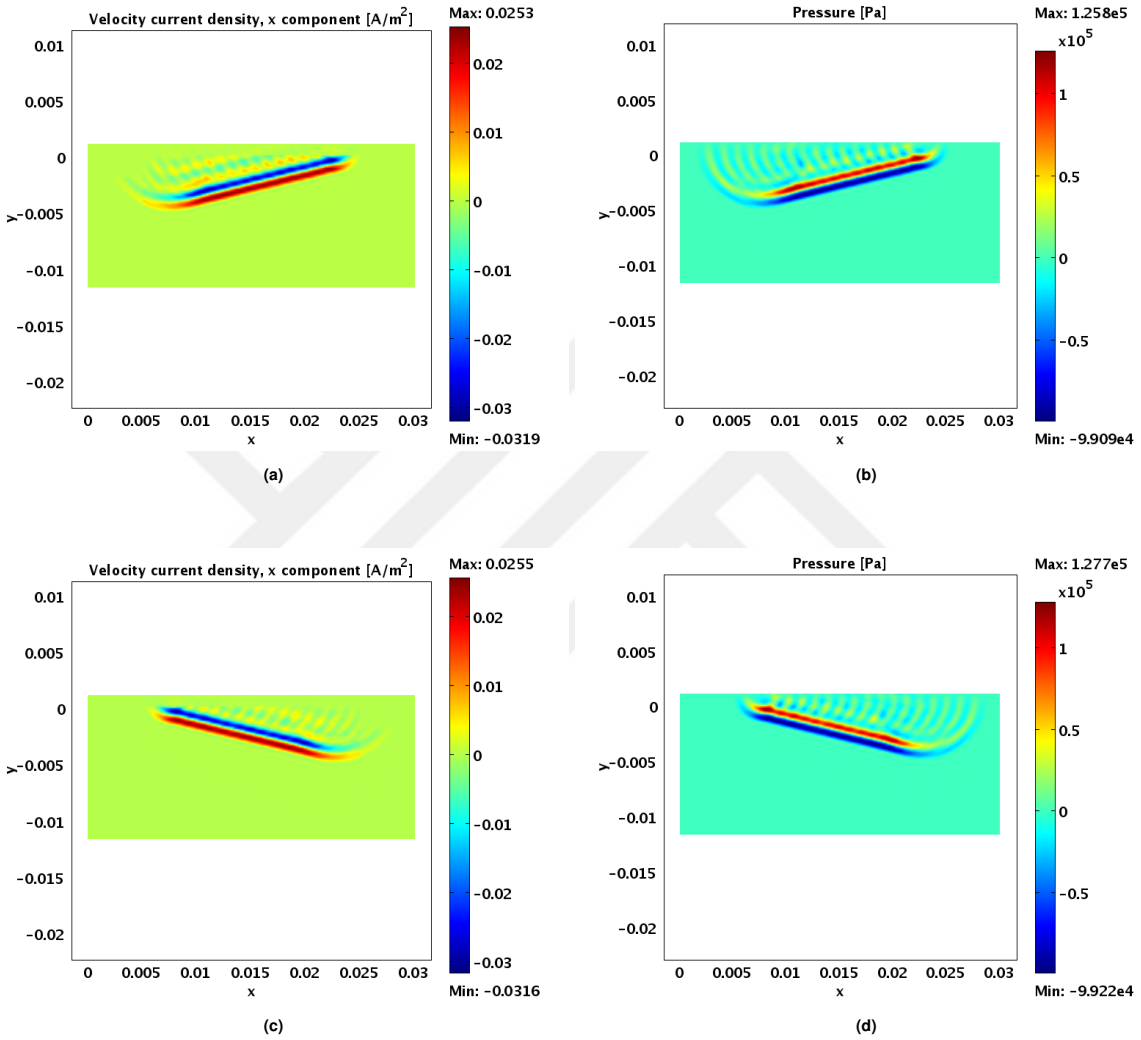


Figure 3.14 Current density (**a, c**) and pressure (**b, d**) distributions in the middle of the wound area for a 16-element LPA transducer driven with 100 V and a full signal (t = 4 μs) at -20 degree (**a, b**) and $+20$ degree (**c, d**) orientations.

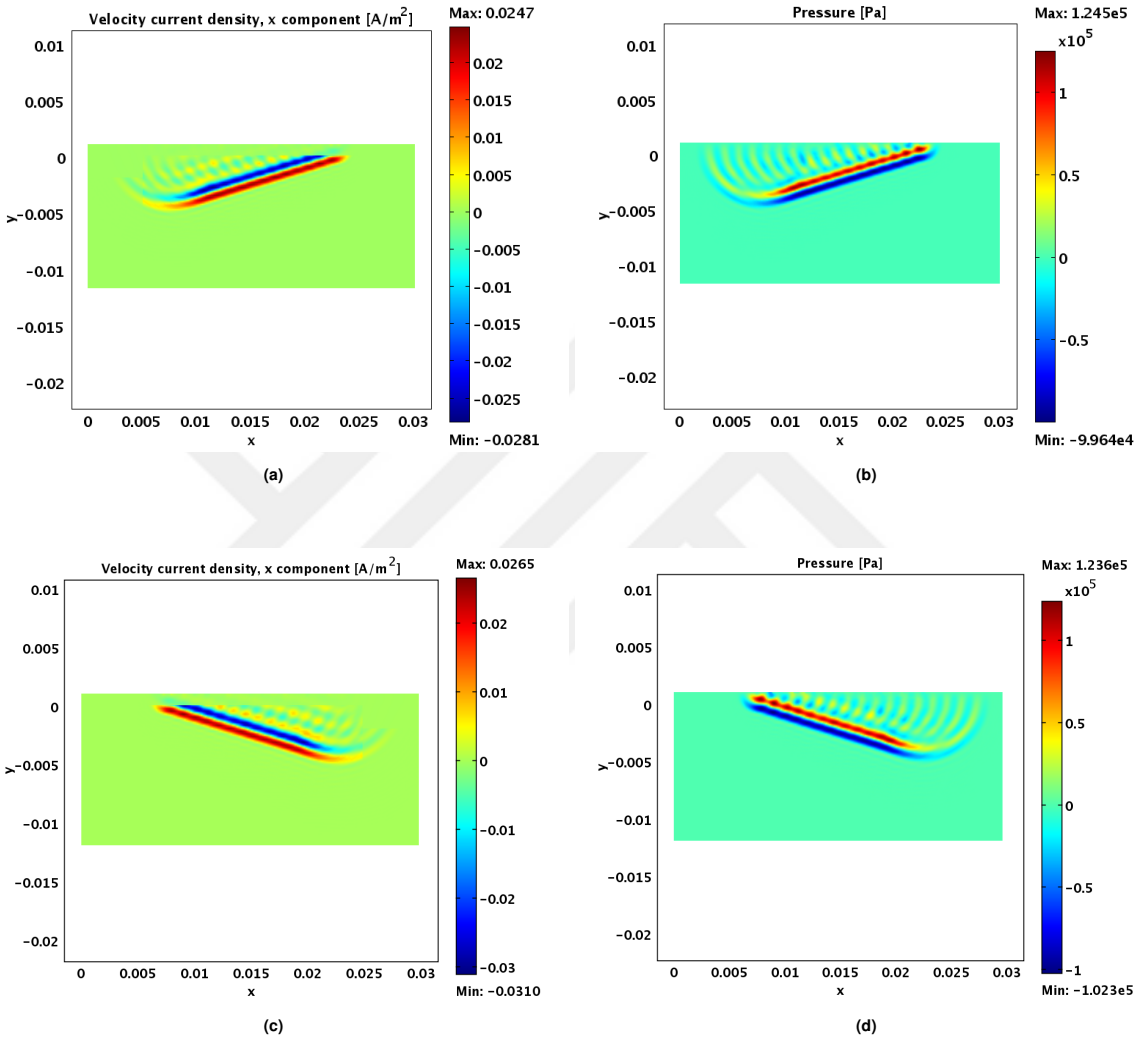


Figure 3.15 Current density (**a, c**) and pressure (**b, d**) distributions in the middle of the wound area for a 16-element LPA transducer driven with 100 V and a full signal (t = 4 μs) at -25 degree (**a, b**) and $+25$ degree (**c, d**) orientations.

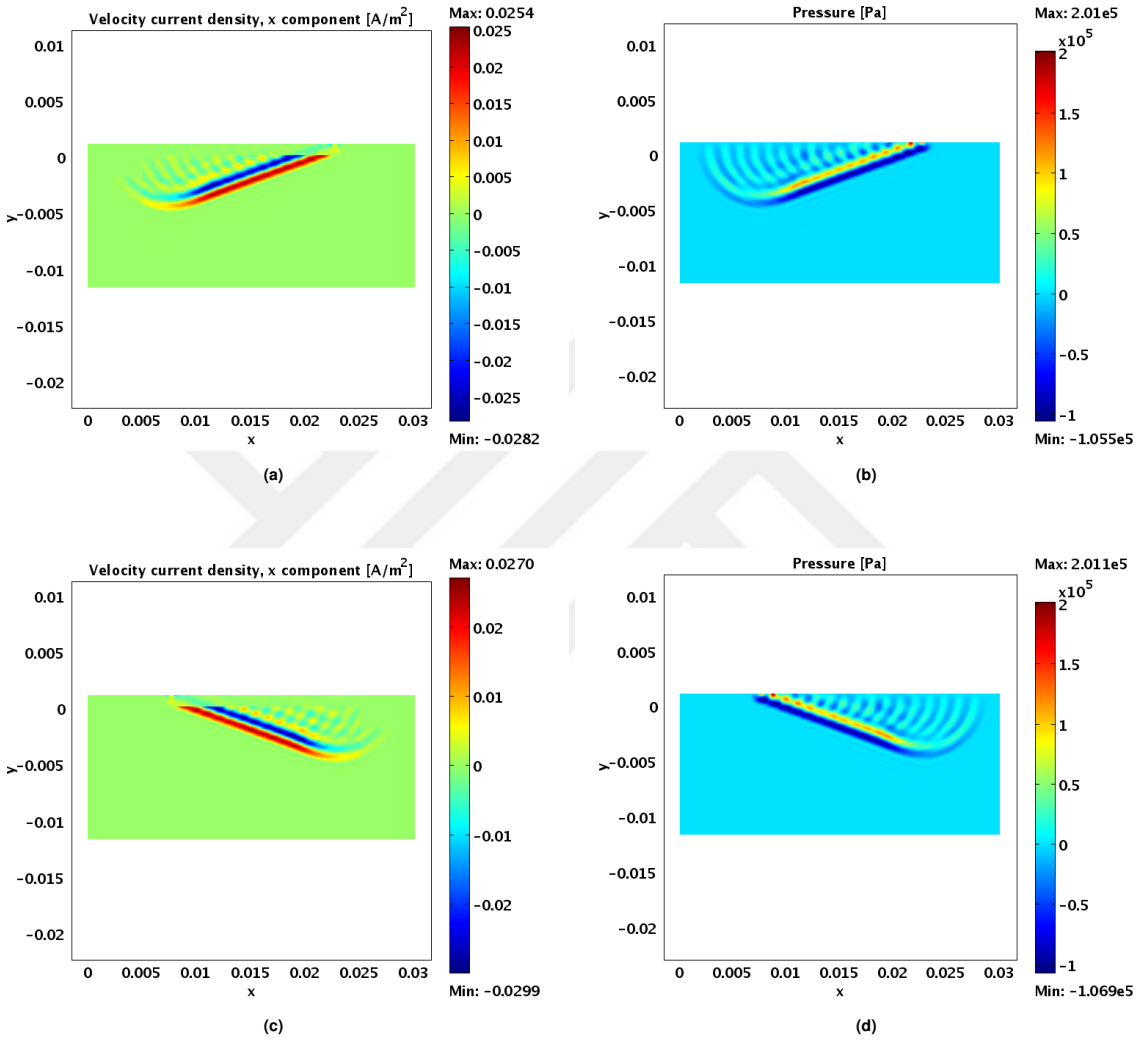


Figure 3.16 Current density (**a, c**) and pressure (**b, d**) distributions in the middle of the wound area for a 16-element LPA transducer driven with 100 V and a full signal (t = 4 μs) at -30 degree (**a, b**) and $+30$ degree (**c, d**) orientations.

Degree	Time (μs)	Velocity Current Density (A/m^2)	Pressure (Pa)
0	4	0.0267	1.19e5
5	4	0.0251	1.18e5
-5	4	0.0232	1.19e5
10	4	0.0238	1.25e5
-10	4	0.0262	1.18e5
15	4	0.0263	1.32e5
-15	4	0.0254	1.24e5
20	4	0.0255	1.28e5
-20	4	0.0253	1.26e5
25	4	0.0146	1.15e5
-25	4	0.0247	1.24e5
30	4	0.0270	2.01e5
-30	4	0.0254	2.01e5

Table 3.2 : Current density distribution in the center of the wound region of a 16-element LPA transducer driven by a 100 V signal between -30 and $+30$ steering angles.

3.7.4 Results from different focusing angles

To examine the electrical potential, pressure, and current density values in the center of the wound, the pressure distribution in the 2D wound model was focused and directed to the desired location. By focusing the pressure distribution on a specific region, changes in the current density in that region have also been observed. The results are shown in the Table 3.3.

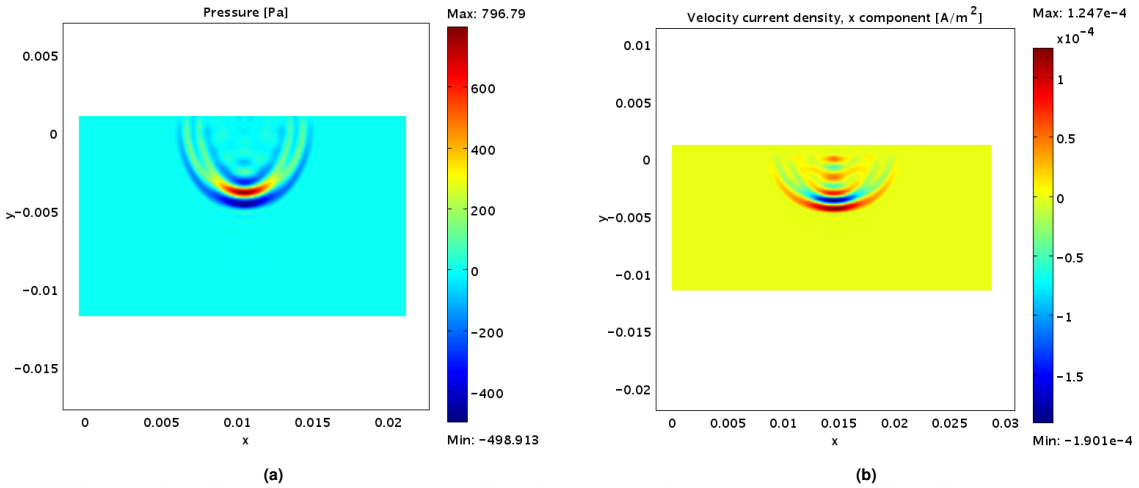


Figure 3.17 a) Pressure distribution and **b)** current density in the center of the wound area when a 100 V signal is applied using two crystals of a 16-element LPA transducer (t=4 μs).

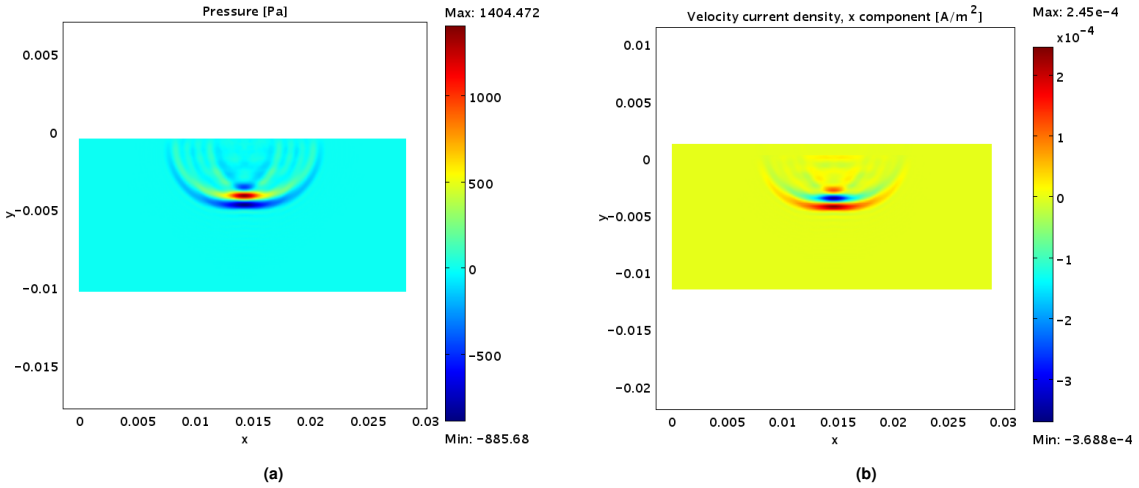


Figure 3.18 a) Pressure distribution and **b)** current density in the center of the wound area when a 100 V signal is applied using four crystals of a 16-element LPA transducer (t=4 μs).

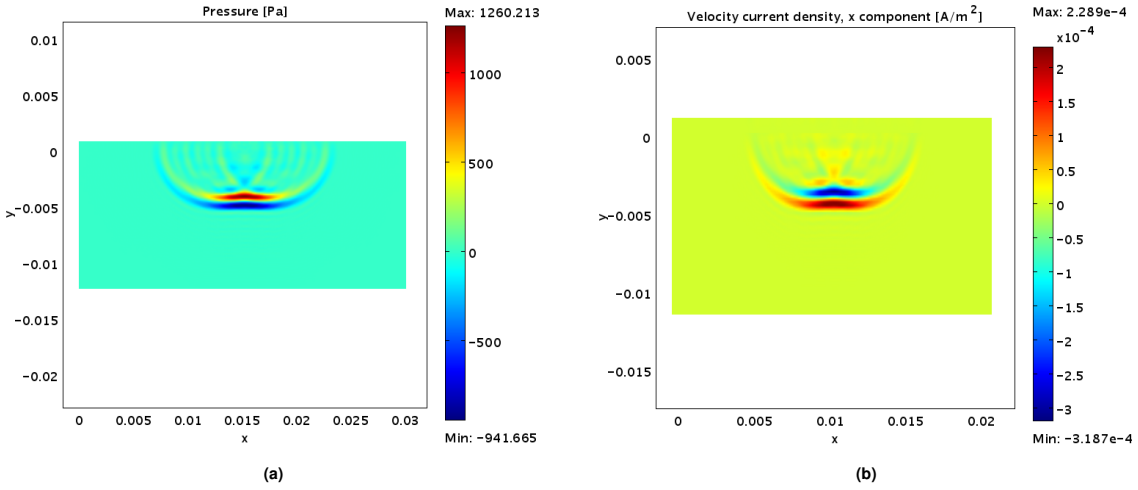


Figure 3.19 a) Pressure distribution and **b)** current density in the center of the wound area when a 100 V signal is applied using six crystals of a 16-element LPA transducer (t=4 μs).

Number of Crystals Focused	Time (μs)	Velocity Current Density (A/m^2)	Pressure (Pa)
2	4	1.90e-4	796.79
4	4	3.68e-4	1404.472
6	4	3.18e-4	2201.878

Table 3.3 : The absolute value distribution of the current density in the center of the winding region is focused by a 16-element LPA converter driven by a 100 V signal.

Numerical studies using the focusing method showed an absolute increase in current density and pressure values at the center of the wound. The Focusing method showed an increase in pressure and current density at the center of the wound compared to the Steering method.

4. STUDIES OF ANIMAL EXPERIMENTS

4.1 Preparation for Experimental Studies

This chapter presents the first experimental demonstration of the wound healing method using ultrasound, static magnetic fields, and Lorentz fields. Building on the numerical findings detailed in Section 3, the hybrid method's initial experimental applications have been implemented to validate and reinforce these results. This thesis marks a pioneering study in the literature, as it uniquely combines numerical analysis with experimental methodologies for this approach to wound healing.

The experimental setup, specifically designed for animal studies, is shown in Figure 4.1. The system consists of Helmholtz coils, permanent magnets, an ultrasonic transducer, and an RF amplifier that powers the transducer in coordination with a signal generator. A detailed description of each component in this experimental configuration is provided below.

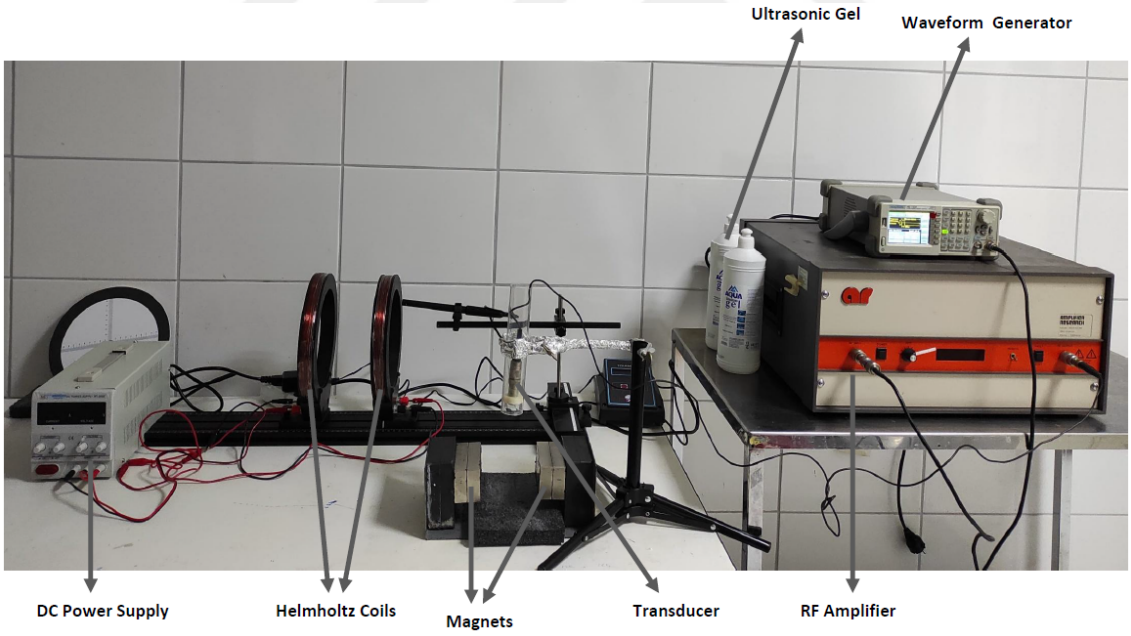


Figure 4.1 : Experiment setup photo. The DC power supply powers the Helmholtz coils. Helmholtz coils and magnets are used to generate a static magnetic field. An RF amplifier and a waveform generator drive an ultrasonic transducer to generate acoustic pressure.

4.1.1 Static magnetic field

Two methods were used to generate a static magnetic field: 1) Permanent magnets and 2) Helmholtz coils. The effect of these static magnetic fields will be monitored individually to assess their influence on wound healing. The intensity of the static magnetic fields applied in this study remains within the safety limits outlined in the guidelines published by ICNIRP in 2009 [98].

Helmholtz Coils: Helmholtz coils consist of two identical coils with a diameter of 18 cm as shown in Figure 4.2. It is aimed to generate a uniform static magnetic field with Helmholtz coils. DC power supply was used to drive the Helmholtz coils with a current of 2 A. As can be seen in Figure 4.3, a uniform magnetic field of approximately 3.2 mT was generated. This magnetic field is within safe limits [98].

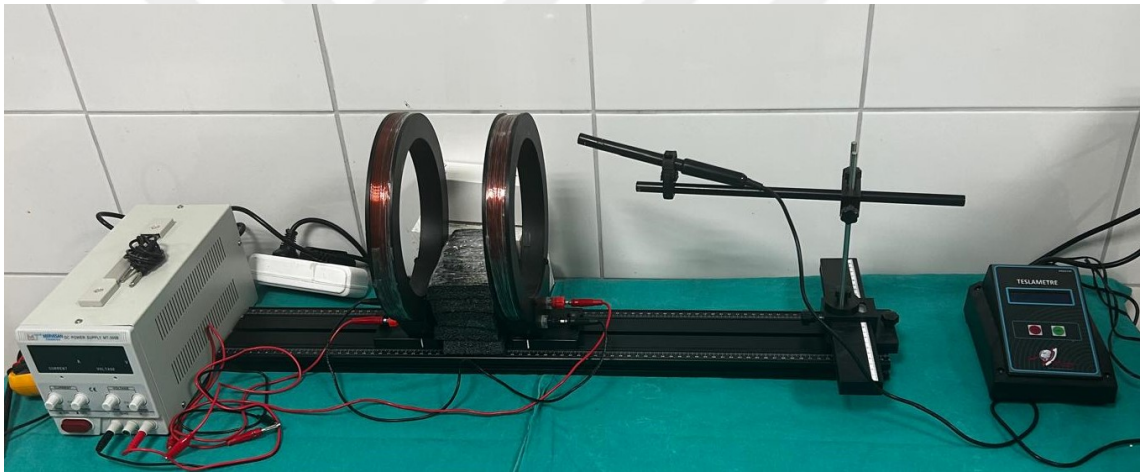


Figure 4.2 : Helmholtz coil pairs model with DC power supply and a Tesla meter.

When the Helmholtz coil assembly was set up, the distance between the two coils was adjusted according to the distance at which the static magnetic field would be maximum. As seen in Figure 4.3, since the radius is set to 9 cm, the maximum static magnetic field value should be between 3.4 mTesla and 3.6 mTesla. After the experimental setup, the value of the static magnetic field was measured to be about 3.2 mTesla as shown in Figure 4.4.

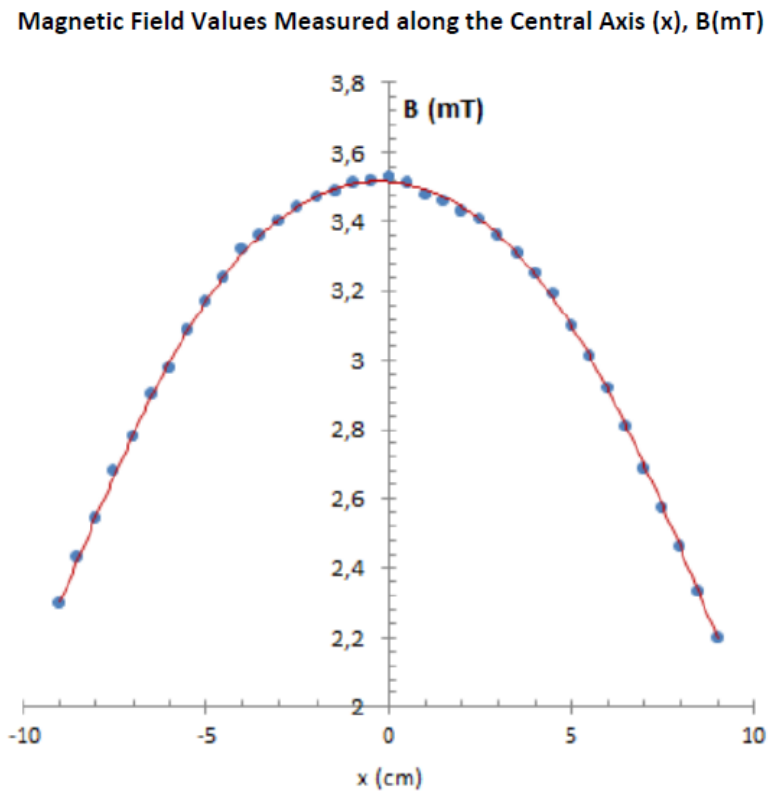


Figure 4.3 : Variation of Magnetic Field on the Central Axis according to Distance [99].

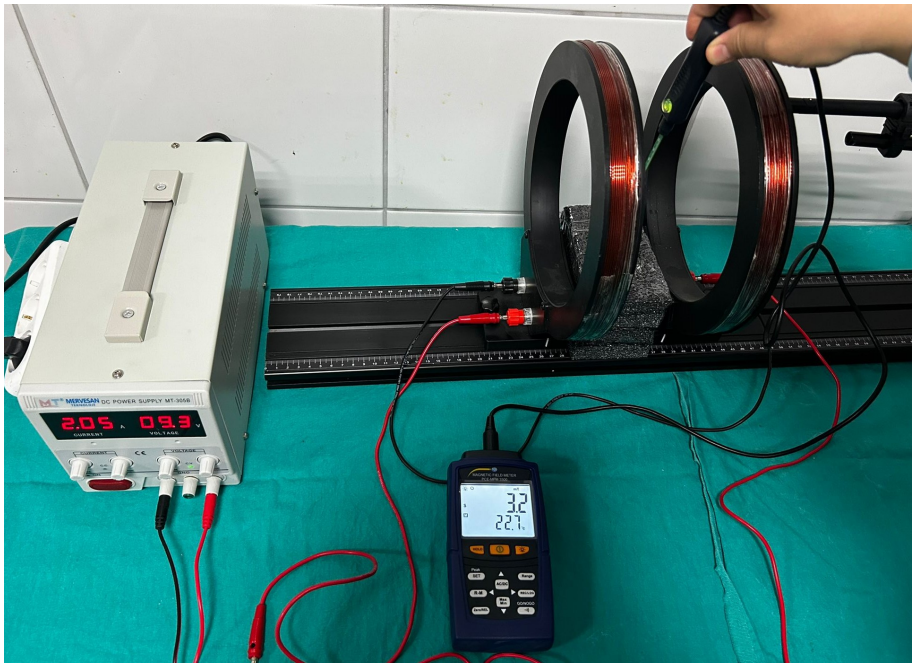


Figure 4.4 : Measurement of static magnetic fields utilizing Helmholtz coils with Gaussmeter.

Permanent Magnets: Neodymium (permanent) magnets with dimensions of $100\ mm\ x\ 50\ mm\ x\ 20\ mm$ were used to obtain static magnetic field. The value of the static magnetic field generated with permanent magnets is higher than that generated with Helmholtz coils. The numerical analysis of static magnetic field generation with permanent magnets is conducted with Comsol Multiphysics, and a line graph of static magnetic field distribution in the middle of the magnets is seen in Figure 4.5. The measurements of static magnetic fields near the magnets and in the middle of the magnets, taken with a Gaussmeter, are presented in Figure 4.6. As shown in this figure, the maximum value of the static magnetic field is 421 mTesla, recorded close to the magnets, while the minimum value of 123 mTesla is found in the middle of the magnets.

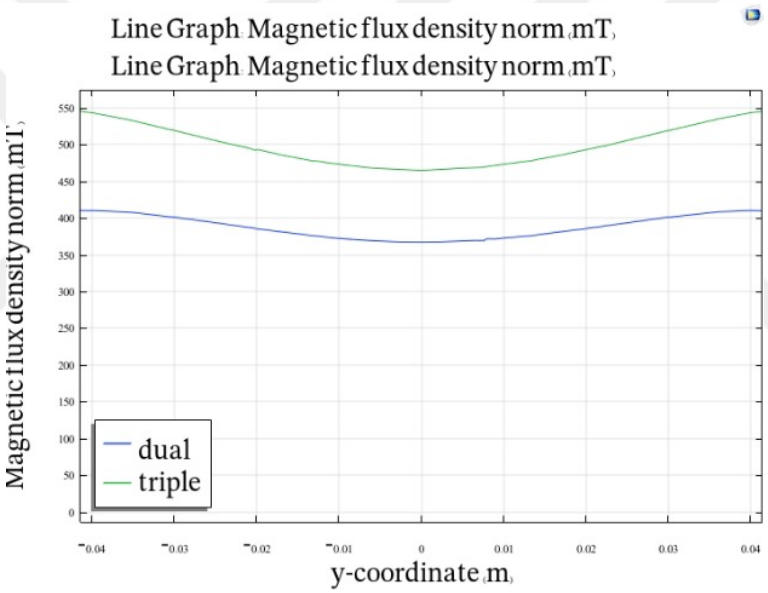


Figure 4.5 : Line graph of magnetic flux density for each permanent magnet pair between the magnets

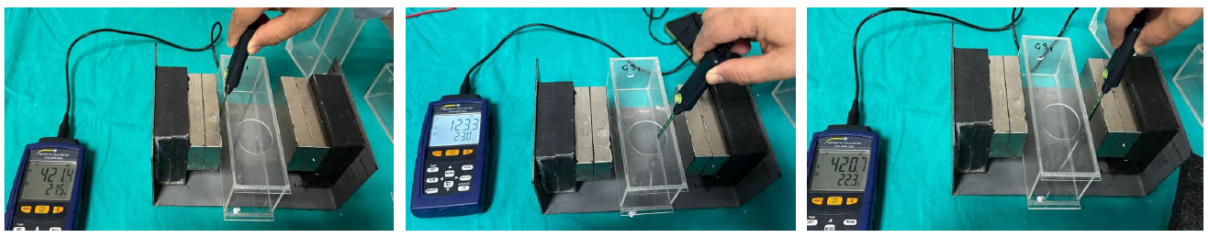
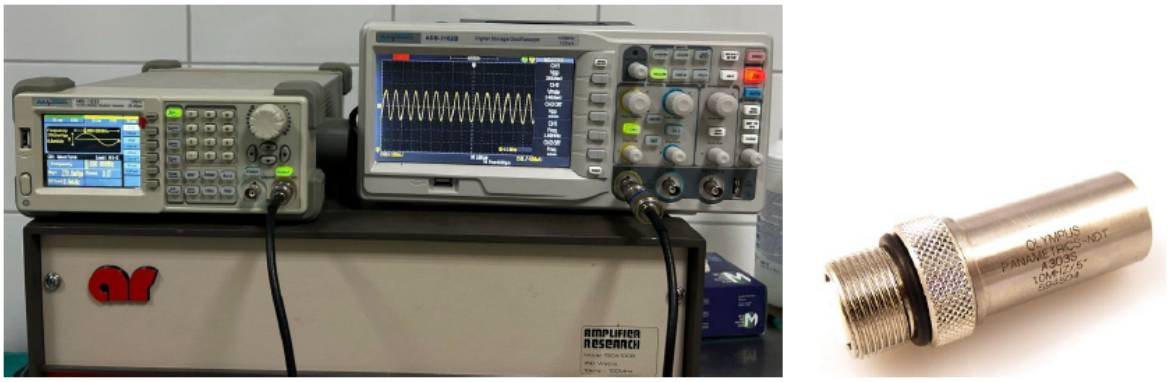


Figure 4.6 : Permanent Magnets Measurements. a) Nearby the left magnet. The magnetic flux density is 421.4 mTesla. b) At the center of magnets. The magnetic flux density is 123.3 mTesla. c) Nearby the right magnet. Magnetic flux density is 420.7 mTesla.

4.1.2 Ultrasonic transducer

In this study, a single-element ultrasonic transducer is used to generate acoustic waves. To drive the ultrasonic transducer, an RF amplifier and a waveform generator were employed. The RF amplifier enhances the signal from the waveform generator by a factor of 37, producing a sinusoidal signal on the probe. The numerical studies were conducted using a sinusoidal signal with an amplitude of 100 V_{pp}. To achieve this, the waveform generator was set to generate a 270 mV_{pp} signal at a frequency of 1 MHz. Consequently, the RF amplifier amplifies the 270 mV_{pp} signal from the waveform generator to yield nearly a 100 V_{pp} output (270 mV_{pp} x 37≈100 V_{pp}). The configuration of the ultrasonic transducer circuit is illustrated in Figure 4.7.



(a) (b)

Figure 4.7 : Ultrasonic Experiment Model. a)RF amplifier, Waveform Generator, and Oscilloscope measurements. b) A single-element immersion transducer, Olympus Accuscan A303S-SU.

4.1.3 Lorentz Fields

A Lorentz electric field is generated in the wound area by applying an ultrasonic transducer within a static magnetic field. Given the conductive nature of the wound tissue, a corresponding current density develops in this region. This current density is anticipated to facilitate the acceleration of the healing process. In the present study, permanent magnets are utilized to establish the static magnetic field, while an ultrasonic transducer is implemented to deliver ultrasonic treatment. The equation governing the Lorentz electric field is thoroughly elaborated upon in the Mathematical Background section. Additionally, a visual representation of the Lorentz field model is provided in Figure 4.8.

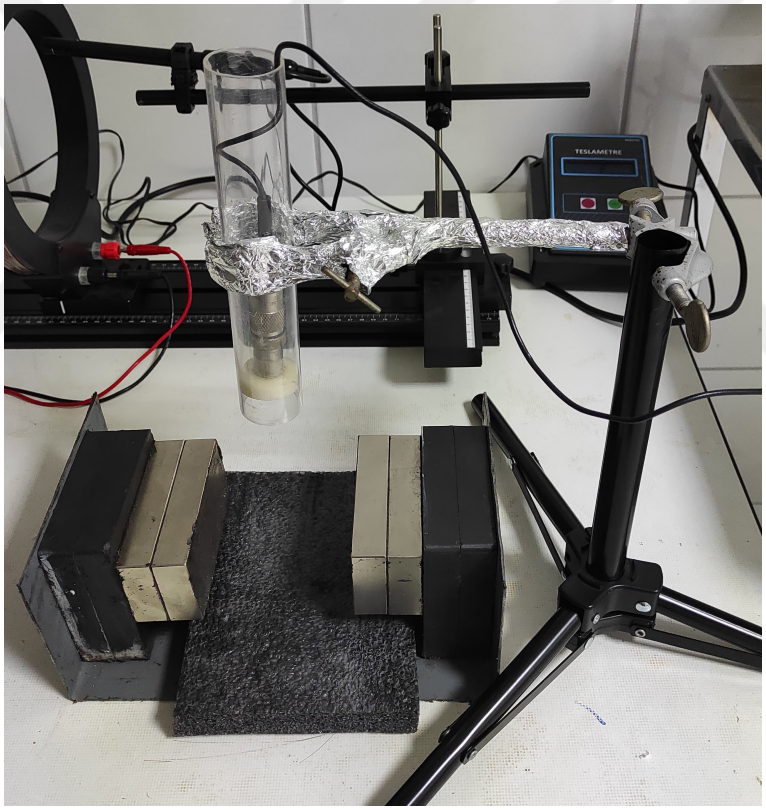


Figure 4.8 : Lorentz Field Experiment Model. It consists of permanent magnets and an ultrasonic transducer.

4.2 Results of Animal Experiments

Animals

Animal experiments were carried out between October 15, 2024, and October 28, 2024, at Inonu University Experimental Animal Production and Research Center within the scope of the project of TÜBİTAK 122E150 with ethical approval numbered 2021/9-3. In this study, 32 male Albino Wistar rats aged 4 months, approximately 320-330 g were used. These rats were divided into four groups, eight in each group: 1) static magnetic field (divided into the permanent magnet and Helmholtz coils), 2) ultrasound, 3) Lorentz field (hybrid method), and 4) control group. During the study, rats were housed in individual cages with one (1) rat in each cage, with appropriate lighting (12 hours light/12 hours dark) and room temperature (22±2ºC). Rats were fed with standard rat chow until the end of the study. The cages were cleaned weekly.

Experimental Groups

The rats to be used in this study were divided into 4 groups. 1^{th} *Group Static Magnetic Field:* This group was divided into two permanent magnets and Helmholtz coils. 4 rats were treated with the permanent magnets in Figure 4.6 and 4 rats were treated with Helmholtz coils in Figure 4.2. 2^{nd}*Group Ultrasound:* There are 8 rats in this group. This group was treated with the ultrasonic transducer in Figure 4.7. 3^{rd} *Group Lorentz Field:* There are 8 rats in this group. This group was treated with the Lorentz experimental setup in Figure 4.8. 4^{th}*Group Control Group:* There are 8 rats in this group. After the wounds of the rats in this group were generated, no treatment was performed.

Anesthesia of Rats

A combination of 10mg/kg Xylazine (Rompun 2 %) and 100mg/kg Ketamine (Keta-Control) was injected intramuscularly to anesthetize the rat.

Wound Formation

For wound formation, the back of anesthetized rats was shaved with a shaver. The area was first cleaned with 10% povidine iodine and then with 70% ethyl alcohol. Then, a 2 cm x 2 cm x 0.5 cm wound was formed on the back of each rat by measuring with a ruler.

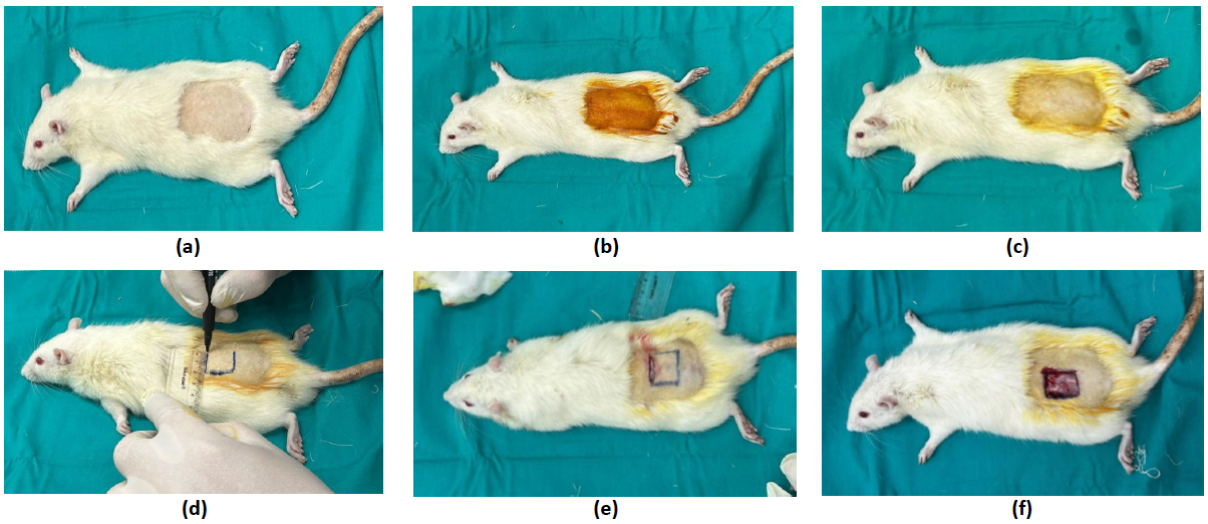


Figure 4.9 : Stages of skin wound formation in rats used in the study. a) Shaving the selected area of the rat for the wound. b) Applying povidone iodine to the wound site of a rat. c) Cleaning the wound site of the rat with ethyl alcohol. d) Determination of the wound area generated by measuring with a ruler. e) Cutting the wound area after measurement. f) Image of the wound generated.

Experimental Group and Monitoring

Experimental studies were carried out in 4 groups as mentioned above. In the experiment, which began with 32 animals, one rat in the control group did not recover from anesthesia. As a result, while all other groups consisted of 8 animals, the control group included only 7. An overview of all groups is provided in Figure 4.9, with detailed descriptions given below.



Figure 4.10 : Cages housing the rats (n=31) and the rack on which the cages are placed. a) Static Magnetic Field group (n=8), b) Ultrasound group (n=8), c) Lorentz Field group (n=8), d) Control group (n=7).

Group 1: Static Magnetic Field Method

Permanent Magnets Application: In the experiment performed using the permanent magnet method for static magnetic field, 4 animals were applied. A visual of the application method is shown in Figure 4.11. The wound on the back of the rat was positioned near the magnets. The 176 mT magnetic field formed in the center of the setup was applied to each rat for 5 minutes per day during the experimental period.

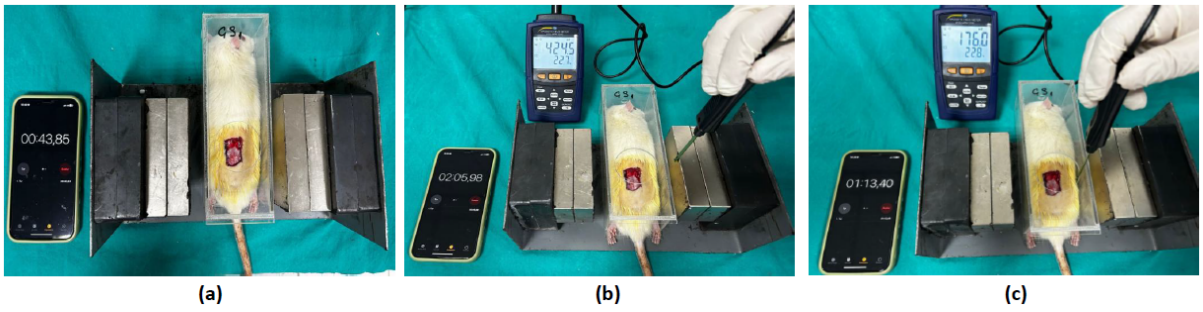


Figure 4.11 : Application with permanent magnets. a) Measurement of the magnetic field at the right edge of the magnet during the application. b) Measurement of the magnetic field at the center of the setup during the application.

Helmholtz Coils Application: In the experiment performed using the Helmholtz coils method for static magnetic field, 4 animals were applied. A visual of the application method is given in Figure 4.12. The wound on the back of the rat was positioned in the center of the coils. A current of 2 A was applied to the coils. This magnetic field was applied to each rat for 5 minutes per day during the experimental period.

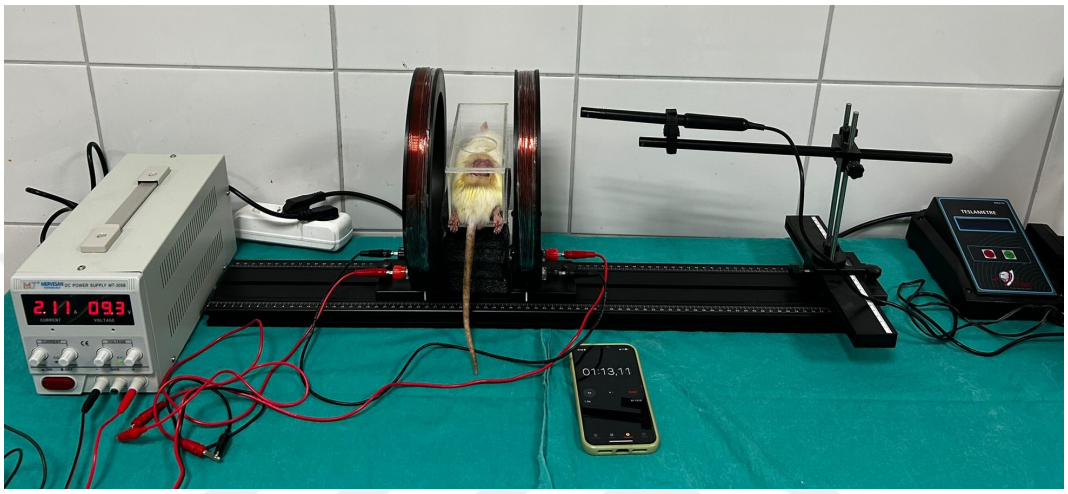


Figure 4.12 : Application with Helmholtz coils.

Group 2: Ultrasound Method

The ultrasonic transducer setup is available in Figure 4.7. The Waveform Generator is set to 270 mV_{pp} at a frequency of 1 MHz. When the RF Amplifier probe is driving the ultrasound, the 270 mV_{pp} signal from the signal generator is amplified 37 times and generates a sinusoidal signal with an amplitude of 100 V_{pp} on the probe. While applying the probe, AQUA Ultrasound Gel was applied between the wound and the probe to transmit the signal more effectively. All rats in this group of 8 rats were treated for 5 minutes a day during the experimental period. The stages of the application are shown in Figure 4.13.

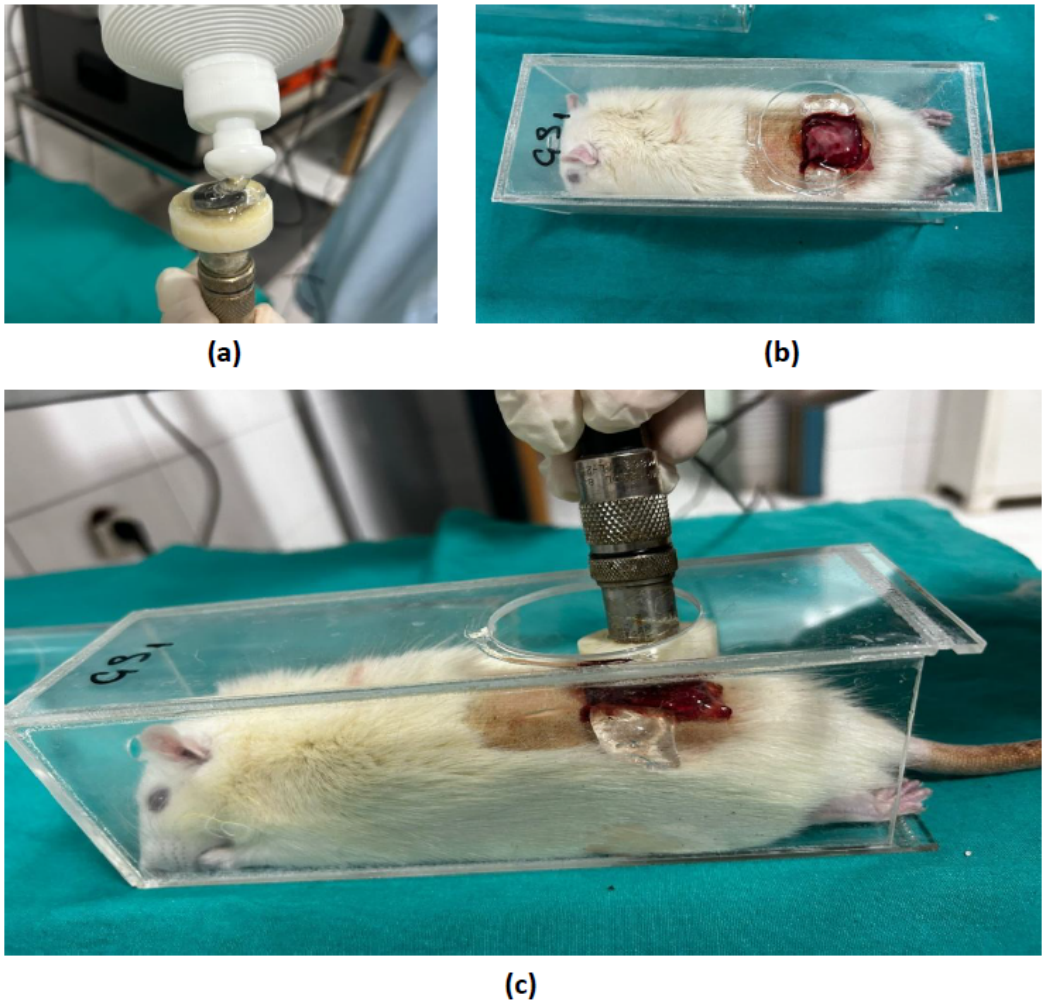


Figure 4.13 : Application with Ultrasound. (a) Ultrasound gel was applied to the transducer. (b) Contact of the ultrasound gel with the wound surface. (c) Application of ultrasound method to the rat.

Group 3: Lorentz Fields

The Lorentz field method combines the magnetic field method and the ultrasound method. In the Lorentz field method, permanent magnets generated the static magnetic field. Each rat was placed in a static magnetic field consisting of permanent magnets. A 270 mV_{pp} signal at a frequency of 1 MHz was tuned from the Waveform Generator. With the RF Amplifier probe, this signal was amplified 37 times to generate a 100 V_{pp} signal. AQUA Ultrasound gel was applied to the tip of the probe and placed on the wound. All rats in this group of 8 rats were treated for 5 minutes a day during the experimental period. The application is shown in Figure 4.14.

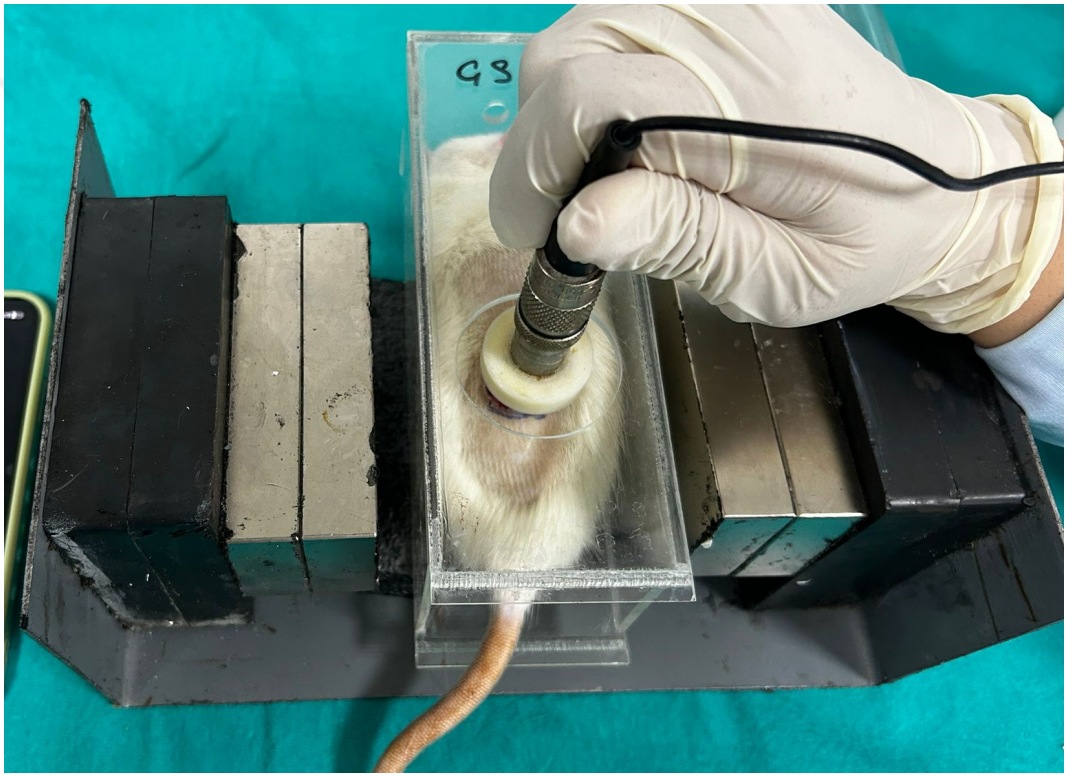


Figure 4.14 : Application of Lorentz Field method to the rat.

Group 4: Control Group

The control group initially consisted of 8 rats. After the anesthesia was given during the wound creation phase, one rat could not wake up. For this reason, 7 rats were placed in their cages after wound formation. No application was made to this group during the experimental period.

Images of Wound Healing Process Measurement by Days

In this study, the effects of static magnetic field, ultrasound, and Lorentz fields on wound healing were investigated. During the experiment, each group was exposed to the mentioned healing methods for 5 minutes per day for 14 days. The first day of wound formation is shown in Figure 4.9. To evaluate the effect of the treatments, measurements were taken with a ruler from the rats in the group following the formation of the wounds. Photographs of the measurements taken on days 3, 6, 9, 12, 13, 14, and 15 are presented in Figure 4.15 to observe the changes in wound size more clearly. When Figure 4.15 is examined, it is observed that the wound sizes decreased most significantly in the Lorentz fields group. This was followed by a decrease in wound size in the ultrasound group and the static magnetic field group. The last change was observed in the control group.



Figure 4.15 : After the wound was generated, measurements were done and photographed on the wounds of the rats in all groups during the 14-day application period.

Results of Wound Healing Process Measurement by Days

Measurements were meticulously recorded from each experimental group over 14 days. The wound size, initially established at 2x2 cm^2, exhibited varying degrees of reduction across the different groups throughout the healing process. Given the asymmetrical nature of wound shrinkage, short and long-side measurements were taken to ensure accuracy. The comprehensive results from all groups are illustrated in Figure 4.16, where the daily average measurements are indicated beneath each respective group. Upon analyzing Figure 4.16, it is evident that the most significant reduction in wound size occurred in the Lorentz fields group. This was followed by the ultrasound group and the static magnetic field group, which demonstrated notable improvements as well. In contrast, the control group exhibited the least change in wound size. Such findings highlight the varying efficacy of the different treatment modalities employed in promoting wound healing.

Wound Healing Measurements by Days																																			
Groups	Rat No	Day 1		Day 2		Day 3		Day 4		Day 5		Day 6		Day 9		Day 12		Day 13		Day 14		Day 15	
		Daily Measurements (cm) (ss)	Daily Measurements (cm) (ls)	Daily Measurements (cm) (ss)	Daily Measurements (cm) (ls)	Daily Measurements (cm) (ss)	Daily Measurements (cm) (ls)	Daily Measurements (cm) (ss)	Daily Measurements (cm) (ls)	Daily Measurements (cm) (ss)	Daily Measurements (cm) (ls)	Daily Measurements (cm) (ss)	Daily Measurements (cm) (ls)	Daily Measurements (cm) (ss)	Daily Measurements (cm) (ls)	Daily Measurements (cm) (ss)	Daily Measurements (cm) (ls)	Daily Measurements (cm) (ss)	Daily Measurements (cm) (ls)	Daily Measurements (cm) (ss)	Daily Measurements (cm) (ls)
Group 1: Static Magnetic Field	1	2	2	2	2	1,9	1,9	1,8	1,9	1,8	1,9	1,6	1,7	1,3	1,4	1	1,2	0,7	1,1	0,5	1,1	0,5	0,9
	2	2	2	2	2	1,9	1,9	1,8	1,9	1,8	1,8	1,6	1,7	1,1	1,2	1	1	0,8	0,9	0,8	0,8	0,7	0,8
	3	2	2	2	2	1,9	1,9	1,8	1,9	1,8	1,8	1,7	1,8	1,5	1,5	1,1	1,4	1	1,2	0,9	1,2	0,7	1,1
	4	2	2	2	2	1,9	1,9	1,8	1,8	1,7	1,8	1,6	1,7	1,4	1,5	1	1,2	0,7	1,1	0,7	1,1	0,5	1
	5	2	2	2	2	1,9	1,9	1,8	1,8	1,7	1,9	1,7	1,7	1,5	1,5	1,2	1,3	1	1,3	0,9	1,3	0,7	1,1
	6	2	2	2	2	1,9	1,9	1,9	1,9	1,7	1,9	1,8	1,8	1,5	1,8	1	1,2	0,8	1,2	0,8	1,2	0,5	1
	7	2	2	2	2	1,9	1,9	1,8	1,8	1,7	1,8	1,6	1,8	1,5	1,7	1,2	1,5	1	1,2	0,8	1	0,7	1
	8	2	2	2	2	1,9	1,9	1,9	1,9	1,8	1,8	1,7	1,8	1,6	1,8	1,2	1,2	0,9	1	0,8	1	0,7	0,7
	Mean±SE	2	2	2	2	1,9	1,9	1,8375	1,8625	1,75	1,8375	1,65	1,75	1,425	1,55	1,0875	1,25	0,8625	1,125	0,775	1,0875	0,625	0,95
Group 2: Ultrasound	1	2	2	2	2	1,8	1,8	1,7	1,7	1,5	1,6	1,3	1,5	1	1,1	0,5	1	0,5	0,8	0,5	0,8	0,4	0,7
	2	2	2	2	2	1,8	1,8	1,7	1,8	1,6	1,6	1,5	1,6	1,3	1,5	1	1,2	0,9	1,1	0,7	1,1	0,5	1
	3	2	2	2	2	1,8	1,8	1,7	1,8	1,5	1,6	1,3	1,4	1	1,3	0,7	1	0,5	0,8	0,5	0,8	0,3	0,6
	4	2	2	2	2	1,8	1,8	1,6	1,7	1,6	1,6	1,5	1,5	1	1	0,4	0,8	0,5	0,8	0,4	0,8	0,4	0,7
	5	2	2	2	2	1,8	1,8	1,7	1,7	1,5	1,6	1,3	1,4	1,1	1,3	0,8	0,9	0,5	0,7	0,4	0,7	0,4	0,6
	6	2	2	2	2	1,8	1,8	1,7	1,7	1,5	1,6	1,3	1,5	1	1,4	0,8	0,9	0,5	0,8	0,5	0,8	0,4	0,7
	7	2	2	2	2	1,8	1,8	1,6	1,7	1,5	1,5	1,2	1,3	1	1,4	0,6	1,2	0,4	1	0,4	1	0,4	1
	8	2	2	2	2	1,8	1,8	1,7	1,7	1,5	1,5	1,4	1,5	1,3	1,3	1	1,2	0,9	1	0,8	1	0,7	0,8
	Mean±SE	2	2	2	2	1,8	1,8	1,675	1,725	1,525	1,575	1,35	1,4625	1,0875	1,2875	0,725	1,025	0,5875	0,875	0,525	0,85	0,4375	0,7625
Group 3: Lorentz Field	1	2	2	2	2	1,7	1,7	1,5	1,6	1,3	1,6	1,2	1,4	0,9	1	0,8	1	0,8	0,9	0,8	0,9	0,4	0,5
	2	2	2	2	2	1,7	1,7	1,7	1,7	1,5	1,6	1,3	1,6	1,1	1,3	0,9	1	0,7	0,8	0,7	0,8	0,6	0,6
	3	2	2	2	2	1,7	1,7	1,7	1,7	1,5	1,6	1,2	1,5	0,8	1,1	1	1	0,7	0,8	0,6	0,8	0,6	0,7
	4	2	2	2	2	1,7	1,7	1,5	1,5	1,4	1,5	1,1	1,3	1	1,2	0,8	0,9	0,4	0,7	0,4	0,6	0,3	0,6
	5	2	2	2	2	1,7	1,8	1,6	1,8	1,5	1,6	1,5	1,5	1	1,3	0,8	1,1	0,7	0,8	0,4	0,7	0,4	0,6
	6	2	2	2	2	1,7	1,7	1,5	1,5	1,3	1,3	1,1	1,2	1	1,1	0,9	1	0,9	1	0,7	0,9	0,5	0,6
	7	2	2	2	2	1,8	1,8	1,7	1,8	1,5	1,6	1,2	1,5	0,8	1,4	0,5	0,7	0,5	0,7	0,4	0,7	0,3	0,7
	8	2	2	2	2	1,7	1,7	1,7	1,7	1,5	1,6	1,2	1,5	0,7	1,4	0,4	1	0,3	1	0,3	1	0,3	0,9
	Mean±SE	2	2	2	2	1,7125	1,725	1,6125	1,6625	1,4375	1,55	1,225	1,4375	0,9125	1,225	0,7625	0,9625	0,625	0,8375	0,5375	0,8	0,425	0,65
Group 4: Control Group	1	2	2	2	2	2	2	1,9	2	1,9	2	1,8	1,9	1,4	1,6	1,2	1,3	1	1,2	0,8	0,8	0,7	0,8
	2	2	2	2	2	2	2	1,9	2	1,9	2	1,8	1,9	1,5	1,7	1,2	1,4	1	1,1	0,9	1	0,8	1
	3	2	2	2	2	2	2	1,9	2	1,8	1,9	1,7	1,7	1,1	1,5	0,8	1,2	0,7	1	0,6	1	0,6	1
	4	2	2	2	2	2	2	2	2	1,8	1,9	1,8	1,9	1,8	1,8	1,6	1,8	1,5	1,8	1,2	1,6	1,2	1,4
	5	2	2	2	2	2	2	1,9	1,9	1,8	1,9	1,7	1,8	1,5	1,5	0,9	1,3	0,8	1	0,7	1	0,7	1
	6	2	2	2	2	2	2	2	2	1,9	2	1,9	2	1,5	1,6	1,4	1,6	1	1,4	0,9	1,4	0,9	1,4
	7	2	2	2	2	2	2	2	2	1,9	2	1,8	1,9	1,5	1,5	0,9	1	0,8	1	0,7	0,9	0,7	0,8
	Mean±SE	2	2	2	2	2	2	1,9714	1,9857	1,8571	1,9286	1,7857	1,8714	1,4714	1,6000	1,1429	1,3714	0,9714	1,2143	0,8286	1,1000	0,8000	1,0571

Figure 4.16 : Wound measurements for all groups over the 14-day application period following wound formation. The table records the short side (ss) and long side (ls) dimensions of the wounds.

Analysis of Wound Healing Process Measurement Results by Days

The measurement results obtained on the 1st day, 6th day, 9th day and 15th day were then analyzed. As a result of these analyses, it was observed that during the entire experimental period (days 1-15), the LF group showed a statistically significant improvement in short edge and long edge measurements (*$p<0.05$), while the US group showed a lower but significant improvement compared to the LF group. These results suggest that LF application may be an effective method for wound healing and US may support this process. Since all edges of the wound did not shrink equally, short-edge and long-edge measurements were taken as references when preparing the figures. All measurements were compared with the first-day measurement results.

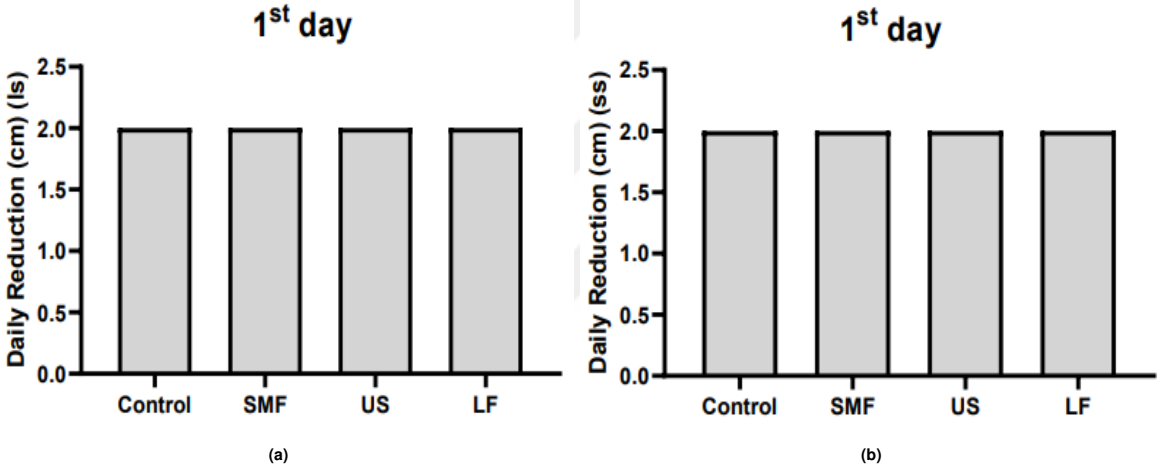


Figure 4.17 On the first day, wound healing rates in all groups were similar at baseline. There was no significant difference in long side (ls) (a) and short side (ss) (b) measurements, and no statistically significant difference was observed between the groups at the beginning of the healing process.

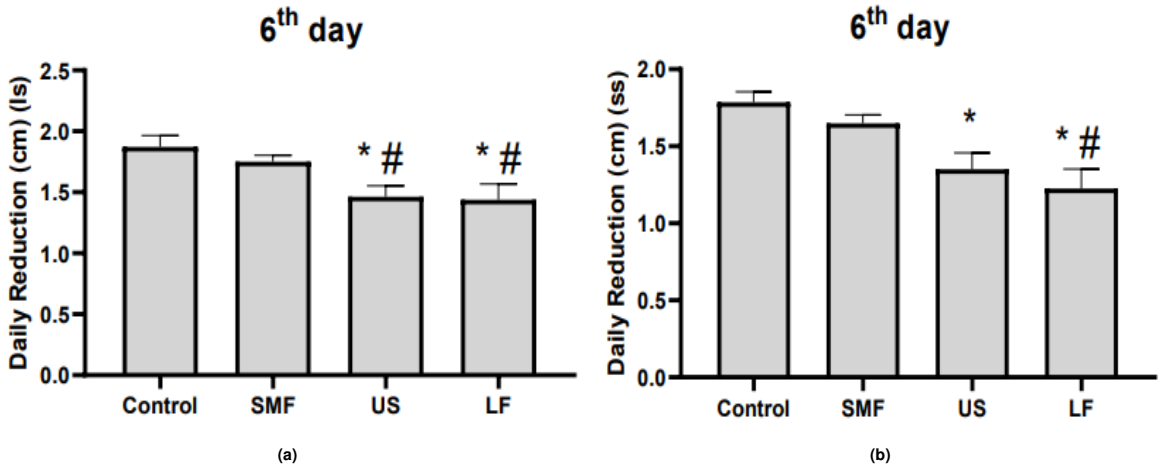


Figure 4.18 Sixth day analyses showed a significant improvement in the healing rates of Lorentz Field (LF) and Ultrasound (US) groups compared to the control and Static Magnetic Field (SMF) groups (*$p<0.05$). It was observed that the healing rate increased in both long side and short side measurements in LF and US groups. This indicates that LF and US applications may accelerate wound healing.

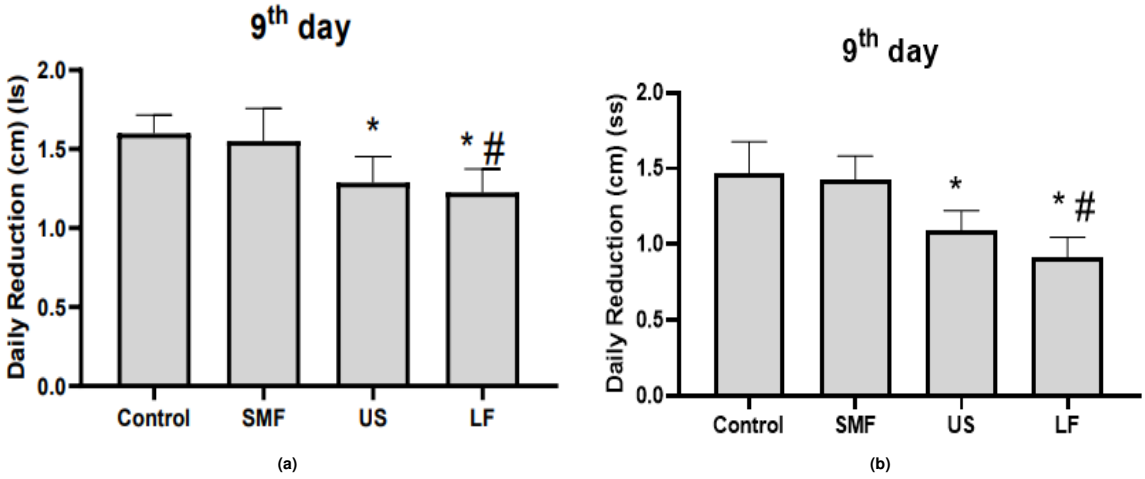


Figure 4.19 Between days 6-9, a statistically significant decrease in short side (ss) measurements was observed especially in the LF group (*$p<0.05$, indicating that the recovery rate was faster compared to the control and SMF groups. Although a similar trend was observed in the US group, a lower effect was observed compared to the LF group. In the SMF group, a slight improvement was observed compared to the control group, but this difference was not significant.

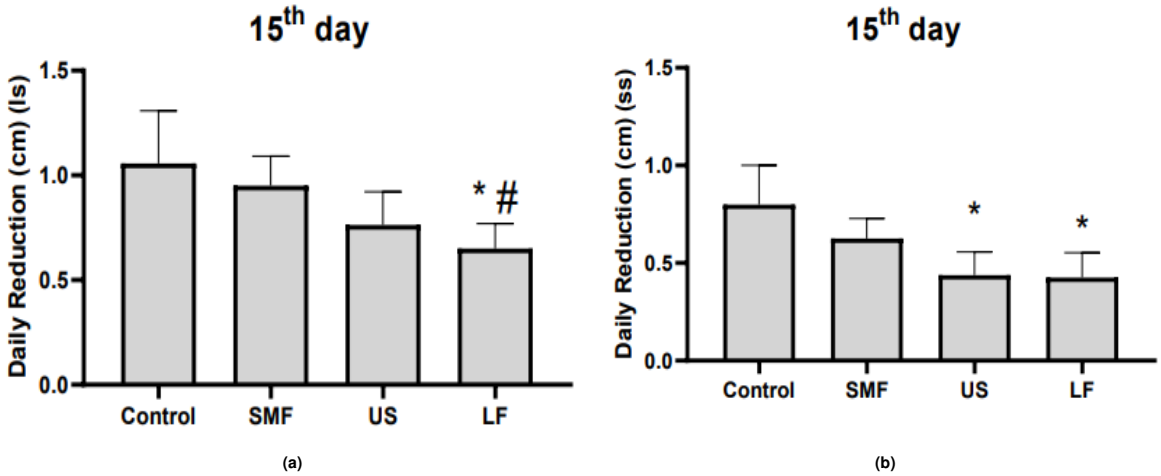


Figure 4.20 The LF group showed the highest healing rate between the 9th and 15th days (*$p<0.05$ and a significant reduction was observed especially in the short side (ss) values. The US group also continued to heal during this period, but showed a lower effect than the LF group. The SMF group tends to improve, although it does not make a statistically significant difference compared to the control group.

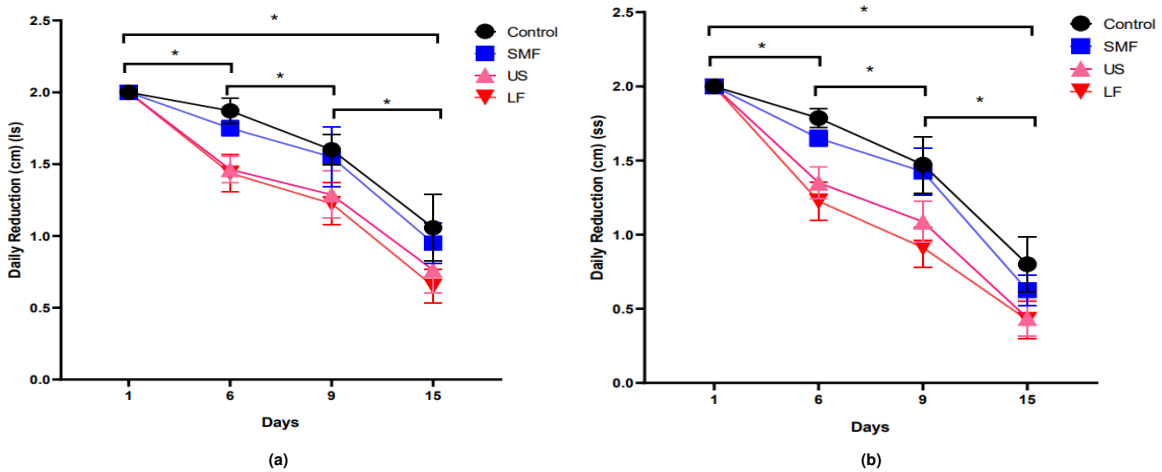


Figure 4.21 During the entire experimental period (days 1-15), statistically significant improvement was observed in the short side and long side measurements in the LF group (*$p<0.05$), while the US group showed a lower but significant improvement compared to the LF group. These results suggest that LF application may be an effective method in wound healing and US may support this process.

5. DISCUSSION AND CONCLUSION

This thesis proposes a new method to accelerate wound healing. This method is based on Lorentz fields generated by ultrasound-induced magnetic fields. The characteristics of the proposed approach are revealed by leveraging the multiphysics properties (acoustic, piezoelectric, and electromagnetic) involved in its different stages. Fundamental field equations governing the behavior of time-varying acoustic and electromagnetic fields are utilized. The resulting pressure variations and current density are analyzed. The effect of different angles of orientation on healing has been observed. This thesis investigates the effects of Lorentz fields on the healing process of chronic wounds. It explores the effects on parameters through various modeling. A realistic skin wound, consisting of layers of skin, wound, ultrasonic transducer, and air, has been modeled in detail. This model allows for a more realistic evaluation of the effect of Lorentz fields on wound healing. The study determined how different angle orientations affect electric potential and current density. Further research is needed to understand how these findings translate into clinical practice and their impact on patients. Additionally, it is essential to consider individual differences and long-term effects. Comments and discussions on different phases of this study are listed below.

Mathematical Modeling: This thesis has a hybrid method that involves multiphysics problems. Therefore, electromagnetic and acoustic fields need to be solved simultaneously. The mathematical background includes electromagnetic and acoustic equations. *Electromagnetic field equations* are given in section 2.1. Electromagnetic fields are calculated as time-varying using Maxwell's equations. *Basic acoustic field equations* to simplify our analysis, let us assume a source-free and lossless environment. Initially, we consider a one-dimensional (1D) scenario. In the static case, the pressure within the body remains constant and is represented by $p0$. The body's mass density $\rho_0(x)$ is considered to be position-dependent.

Numerical Studies: The proposed method for enhancing wound healing involves the generation of Lorentz fields, achieved by applying ultrasound within a static magnetic field environment. To solve the problem numerically, the software COMSOL Multiphysics is used. This software package is designed to analyze and

simulate diverse physics and engineering problems. It utilizes advanced finite element analysis techniques to handle complex multiphysics phenomena and solve partial differential equations [70]. In our problem, the acoustic, piezoelectric, and electromagnetic modules are solved simultaneously. Each module is characterized by specific physics properties with coupling parameters. *Pressure acoustic module* addresses issues in acoustics, acoustic-structure interactions, pressure, vibrations, acoustic fields, and other acoustics-related areas. The Pressure Acoustics Module, located within the Acoustic Module category, analyzes the acoustic properties within each subdomain and evaluates boundary conditions. In this study, only two-dimensional numerical models are used. *The piezoelectric module:* In the piezoelectric module 16-element linear phased array transducer are modeled with PZT-5H material. The inverse piezoelectric effect is performed by exciting each transducer with time-varying electrical potentials. *Electromagnetic module* involves solving Maxwell's equations. Initially, there is only a static magnetic field. When this static magnetic field combines with an acoustic signal, it generates a Lorentz electric field and current density in the tissue.

Animal Experiments:

In this study, animal experiments played a critical role in evaluating the effectiveness of the novel wound healing method utilizing the Lorentz field, ultrasound, and static magnetic field applications. Conducted on four groups—Static Magnetic Field, Ultrasound, Lorentz Field, and a Control group—these experiments provided essential insights into the impact of each treatment on wound healing rates.

Each treatment method demonstrated unique healing effects, with the Lorentz Field group showing promising improvements compared to others. This outcome aligns with theoretical expectations that combining a static magnetic field with ultrasonic stimulation generates a Lorentz electric field, which may promote cellular activities conducive to healing. Furthermore, the different groups allowed for comparative analysis, reinforcing Lorentz Field's enhanced effect in accelerating the wound closure process.

Despite these encouraging results, the ethical considerations associated with animal testing were taken into account, ensuring that experiments were designed and conducted under strict ethical guidelines. The use of a control group and specific

treatment protocols ensured the reliability of the findings while minimizing unnecessary harm to the animals. Future studies might expand on these findings, exploring alternative models or minimizing the use of live animal subjects where possible.

Safety Current Values

IEC 60601-1 (Medical Electrical Equipment) and BS 5724 (British Standard) specify a maximum safe leakage current of 100 μA for electrodes attached to the skin surface and 10 μA for electrodes connected to the heart [89] [90]. Precautions must be taken to ensure that the excitation potential of ultrasound transducers remains below a certain threshold to avoid destructive heating. Ultrasonic transducers designed for diagnostic use do not produce harmful heating effects in the human body [100]. In our simulations, the ultrasonic transducers are activated at a frequency of 1 MHz, which is well within safe limits and does not pose any risk to body tissues. The induced current density in the body should also be under the safety limits. In our simulations, current densities are below the safety limits at 1 MHz [101].

Current Values for Healing Process

After an injury, the process of wound repair begins with the movement of electric charges. This movement results in the formation of an electric current after a few days. These electric fields facilitate the migration of fibroblasts, macrophages, and keratinocytes, which are actively involved in wound healing. The application of the electric field to the wound can either speed up or slow down the healing process. It can be likened to a battery in human skin, with an electric current of 140 mV/mm at the wound edge on the skin of porcine guinea pigs. In humans, the voltage difference between the outermost layer of skin and the dermis has been measured at -23 mV. The hands and feet have a higher skin battery than the back and shoulders. There is a peak current density of 22 $\mu A/cm^2$ after fingertip amputation in children. The skin's pacemaker and electric fields are crucial for wound healing. Reversing the polarity of the physiological electric field when an external electric field is applied delays the wound-healing process. This indicates that the electrodynamic field should be maintained for skin wound healing. Within the first 24-28 hours after injury, the center of the wound becomes positively charged compared to the healthy tissue at its periphery. The electrical potential drops after 24-48 hours, and the wound gradually becomes negatively charged compared to the surrounding tissue. This

lasts for about 8-9 days. Then, the current reaches its maximum value. On the 10th to 12th day after the injury, there is a drop in current values, which return to the original pre-intervention values after the 15th to 16th day. Therefore, wound healing is accompanied by a change in the direction of the electrodynamic field [91].

In a study conducted by Konstantinou et al. [101], it was found that a low direct current of 2 μA increased the growth and migration of fibroblasts into the wound, thereby accelerating wound healing. Similarly, in research by Merriman et al. [102], the application of a direct current ranging from 0.4 to 400 μA was observed to have a bacteriostatic effect, inhibiting bacterial growth during the inflammation phase of the wound. Additionally, in a study by Bourguignon et al. [103], the application of a 50 μA pulsed direct current to the wound for 20 minutes led to an increase in DNA synthesis for fibroblast proliferation during the proliferative phase of the wound. Ex vivo stimulations from as low as 300 μA up to 1 mA have been reported by various groups to show an effect on the inflammatory processes. However, in the case of human skin tissues, the amplitude is found to be much lower, around 10–100 μA, showing a bactericidal effect. Various effects of current stimulation on the proliferation stage of wound healing have been reported in many works which include the increase of fibroblasts, collagen secretion, and migration of epithelial cells. DC stimulations are seen to have ranged from 20 to 300 μA in different works involving the growth and proliferation of fibroblasts. In studies on the treatment of chronic wounds, such as pressure sores, diabetic wounds, and venous ulcers, Wirsing et al. discovered that applying a current of 1.5 μA to a chronic ulcer wound resulted in a reduction of the wound area. The range of applied currents varied from 200 to 800 μA and was found to decrease the wound area [104]. The magnitude of DC stimulation ranges from 200 to 800 μA, contributing to a reduction in wound area [93–97].

In a 2006 study published in Nature [88], using a variety of techniques, consistent and continuous outward electrical currents were confirmed in wounds in human and rodent corneas and skin. A current density of $4 \mu A/cm^2$ was measured at the wound edges of rat cornea and human skin. This current was observed to gradually increase to 10 $\mu A/cm^2$ during the healing process of the wound and then decreased to 4 - 8 $\mu A/cm^2$. It was also observed that the direction and magnitude of the

Table 5.1 : Stimulation parameters having similar effects [104].

Effect	Stimulus parameter
Migration of fibroblast	2 μA DC
	25–100 mV/mm DC
Proliferation of fibroblasts	2 μA DC
	2–100 μA 11 ppm pulsed DC
Antibacterial effect	0.4–400 μA DC
	500 μA DC

current were independent of the wound size. Looking at the current densities in Figures 3.17, 4.21 and 3.19, it can be seen that a current density of approximately 0.27 mA/cm^2 occurs in the wound area, which is sufficient for the wound healing period and also within the safety limits.

Future Work: The following topics can be further investigated:

- Utilization of the proposed approach using other ultrasonic transducers.
- Changing the identified wound type (diabetic foot ulcers, etc.)
- Testing the proposed method in different treatment modalities (e.g. pain relief).
- In this work, the steering and focusing properties of linear phased array and single-element transducers are used to steer electric currents inside a conducting body. The methodology can be further extended to obtain wound treatment modalities. This will certainly increase the effectiveness of the resulting healing data and the proposed method.

REFERENCES

[1] **Arab, A., Orakçı, V., Erbilen, M., Şahin, M.** (1994). Cellular and Molecular Mechanism of Wound Healing. Journal of Turgut Özal Medical Center, 1(2)

[2] **Daunton, C., Kothari, S., Smith, L., Steele, D.** (2012). History materials and practices for wound management. Wound Practice and Research, 20(4), 174–185.

[3] **Erdoğan, B.** (2010). Yara Bakım Ürünleri. In Güncel Yönleriyle Kronik Yara (pp. 143–171)

[4] **Gottrup, F., Leaper, D.** (2004). Wound Healing: Historical Aspects. EWMA Journal, 4(2)(21–7)

[5] **Parsak, C. K., Sakman, G., Çelik, Ü.** (2007). Yara İyileşmesi, Yara Bakımı ve Komplikasyonları. Arşiv Kaynak Tarama Dergisi, 16(2), 145–159.

[6] **Valero, C., Javierre, E., García-Aznar, J. M., Menzel, A., Gómez-Benito, M. J.** (2015). Challenges in the Modeling of Wound Healing Mechanisms in Soft Biological Tissues. Annals of Biomedical Engineering, 43, 1654–1665.

[7] **Ud-Din, S., Bayat, A.** (2014). Electrical Stimulation and Cutaneous Wound Healing: A Review of Clinical Evidence. Healthcare (Basel), 27;2(4), 445–467.

[8] **Wilkinson, H., Hardman, M.** (2020). Wound healing: cellular mechanisms and pathological outcomes. The Royal Society Publishing, 10(9).

[9] **Yalçın, H., Özkalp, B.** (2005). Vücut Hijyeninin Önemi ve Yara Bakımında Yeni Gelişmeler. 4. Ulusal Sterilizasyon Dezenfeksiyon Kongresi.

[10] **Luo, R., Dai, J., Zhang, J., Li, Z.** (2021). Accelerated Skin Wound Healing by Electrical Stimulation. Adv Healthc Mater, 10(16).

[11] **Kloth, L.** (2014). Electrical Stimulation Technologies for Wound Healing. Adv Wound Care (New Rochelle), 1;3(2), 81–90.

[12] **Braun, M., McGrath, A., Downie, F.** (2013) Octenilin range Made Easy. Wounds, 9(4).

[13] **El-Sabbagh, A.** (2017). Negative pressure wound therapy: An update. Chin J Traumatol, 20(2), 103–107.

[14] **Fleischmann, W., Strecker, W., Bombelli, M., Kinzl, L.** (1993). Vacuum sealing as treatment of soft tissue damage in open fractures. Unfallchirurg, 96(9), 488–492.

[15] **Demir, A., Demirtaş, Y., Çifci, M., Öztürk, N., Karacalar, A.** (2006). TOPİKAL NEGATİF BASINÇ (VAKUM YARDIMLI KAPAMA (VAC)) UYGULAMALARIMIZ. Türk Plastik Rekonstrüktif Ve Estetik Cerrahi Dergisi, 14(3), 171–177.

[16] **Bowers, S., Franco, E.** (2020) Chronic Wounds: Evaluation and Management. Am Fam Physician, 101(3), 159–166.

[17] **Moya-López, J., Costela-Ruiz, V., García-Recio, E., Sherman, R., De Luna-Bertos, E.** (2020). Advantages of Maggot Debridement Therapy for Chronic Wounds: A Bibliographic Review. Adv Skin Wound Care, 33(10), 515–525.

[18] **Powers, J. G., Higham, C., Broussard, K., Phillips, T. J.** (2016). Wound healing and treating wounds: Chronic wound care and management. Journal of the American Academy of Dermatology, 74(4), 607–625.

[19] **Zhao, R., Liang, H., Clarke, E., Jackson, C., Xue, M.** (2016). Inflammation in Chronic Wounds. Int J Mol Sci, 17(12), 2085.

[20] **El-Sabbagh, A.** (2017). Negative pressure wound therapy: An update. Chin J Traumatol, 20(2), 103–107.

[21] **Huang, C., Leavitt, T., Bayer, L., Orgill, D.** (2014). Effect of negative pressure wound therapy on wound healing. Curr Probl Surg, 51(7), 301–331.

[22] **Morykwas, M., Argenta, L., Shelton-Brown, E., McGuirt, W.** (1997). Vacuum-assisted closure: a new method for wound control and treatment: animal studies and basic foundation. Ann Plast Surg., 38(6), 553–562.

[23] **Webster, J., Liu, Z., Norman, G., Dumville, J., Chiverton, L., Scuffham, P., Chaboyer, W.** (2019). Negative pressure wound therapy for surgical wounds healing by primary closure. Cochrane Database Syst, 3(3).

[24] **Çelebi, C. R. (n.d.).** Tıbbi ve Cerrahi Yönleriyle Deri Ülserlerinin Debridmanı.

[25] **Balakatounis, K., Angoule, s A.** (2008). Low-intensity electrical stimulation in wound healing: review of the efficacy of externally applied currents resembling the current of injury. Eplasty, 8(e28).

[26] **Zhao, M. (2009).** Electrical fields in wound healing-An overriding signal that directs cell migration. Semin Cell Dev Biol, 20(6), 674–682.

[27] **Ashrafi, M., Alonso-Rasgado, T., Baguneid, M., Bayat, A.** (2016). The efficacy of electrical stimulation in experimentally induced cutaneous wounds in animals. Vet Dermatol, 27(4), 235-e57.

[28] **Mehmandoust FG, Torkaman G, Firoozabadi M, T. G.** (2007). Anodal and cathodal pulsed electrical stimulation on skin wound healing in guinea pigs. J Rehabil Res Dev., 44(4), 611–618.

[29] **Sun, Y.** (2017). Electrical Stimulation for Wound-Healing: Simulation on the Effect of Electrode Configurations. Biomed Res Int.

[30] **Thakral, G., Lafontaine, J., Najafi, B., Talal, T., Kim, P., Lavery, L.** (2013). Electrical stimulation to accelerate wound healing. Diabet Foot Ankle, 16(4).

[31] **Cramp, A. F., Noble, J. G., Lowe, A. S., Walsh, D. M.** (2001). Transcutaneous electrical nerve stimulation (TENS): The effect of electrode placement upon cutaneous blood flow and skin temperature. Acupunct Electrother Res., 26(1–2), 25–37.

[32] **Kaada, B., E, O., Eielsen, O.** (1984). In search of mediators of skin vasodilation induced by transcutaneous nerve stimulation: III. Increase in plasma VIP in normal subjects and in Raynaud's disease. Gen Pharmacol, 15(2), 107–113.

[33] **Nolan, M., Jr Hartsfield, J., Witters, D., Wason, P.** (1993). Failure of transcutaneous electrical nerve stimulation in the conventional and burst modes to alter digital skin temperature. Arch Phys Med Rehabil, 74(2), 182–187.

[34] **Simpson, K., Ward, J.** (2004). A randomized, double-blind, crossover study of the use of transcutaneous spinal electroanalgesia in patients with pain from chronic critical limb ischemia. J Pain Symptom Manage, 28(5), 511–516.

[35] **Wikström, S., Svedman, P., Svensson, H., Tanweer, A.** (1999). Effect of transcutaneous nerve stimulation on microcirculation in intact skin and blister wounds in healthy volunteers. Scand J Plast Reconstr Surg Hand Surg, 33(2), 195–201.

[36] **Ennis, W., Lee, C., Gellada, K., Corbiere, T., Koh, T.** (2016). Advanced Technologies to Improve Wound Healing: Electrical Stimulation, Vibration Therapy, and Ultrasound-What Is the Evidence? Plast Reconstr Surg, 138.

[37] **Ennis, W., Lee, C., Plummer, M., Meneses, P.** (2011). Current status of the use of modalities in wound care: electrical stimulation and ultrasound therapy. Plast Reconstr Surg, 127.

[38] **Ennis, W., Valdes, W., Gainer, M., Meneses, P.** (2006). Evaluation of clinical effectiveness of MIST ultrasound therapy for the healing of chronic wounds. Adv Skin Wound Care, 19(8), 437–446.

[39] **Speed, C. A.** (2001). Therapeutic ultrasound in soft tissue lesions. Rheumatology, 40(12), 1331–1336.

[40] **Sharma, Sahil, Mishra, U. K., Saini, A. K., Dubey, P. K.** (2020). Accuracy Estimation of Propagation Velocity in Variable Path Ultrasonic Interferometer for Liquids. MAPAN, 35, 19–24.

[41] **McCulloch, J. M., Kloth, L. C., Feedar, J. A.** (1995). Wound healing: Alternatives in Management (D. Company, Ed.). Philadelphia

[42] **Michlovitz, S. L.** (1996). Therapeutic Ultrasound (D. Company, Ed.). Philadelphia.

[43] **Hecox, B., Mehreteab, T., Weisberg, J.** (1994). Physical Agents A Comprehensive Textfor Physical Therapist.

[44] **Ovington, L.** (2002). The evolution of wound management: ancient origins and advances of the past 20 years. Home Healthcare Nurse, 20(652), 6.

[45] **Chang, Y., Perry, J., Cross, K. (2017).** Low-Frequency Ultrasound Debridement in Chronic Wound Healing: A Systematic Review of Current Evidence. Plast Surg (Oakv), 25(1), 21–26.

[46] **Doan, N., Reher, A., Meghji, S., Harris, M.** (1999). In vitro effects of therapeutic ultrasound on cell proliferation, protein synthesis, and cytokine production by human fibroblasts, osteoblasts, and monocytes. J Oral Maxillofac Surg, 57, 409–419.

[47] **Ito, M., Azuma, Y., Ohta, T., Komoriya, K.** (2000). Effects of ultrasound and 1,25-dihydroxyvitamin D3 on growth factor secretion in co-cultures of osteoblasts and endothelial cells. Ultrasound Med Biol, 26, 161–166.

[48] **Maxwell, L., Collecutt, T., Gledhill, M., Sharma, S., Edgar, S., Gavin, J.**

(1994). The augmentation of leucocyte adhesion to endothelium by therapeutic ultrasound. Ultrasound Med Biol, 20, 382–390.

[49] **Young, S., Dyson, M.** (1990a). Macrophage responsiveness to therapeutic ultrasound. Ultrasound Med Biol, 16, 809–816.

[50] **Francis, C.** (2001). Ultrasound-enhanced thrombolysis. Echocardiography, 18, 239–246.

[51] **Reher, P., Harris, M., Whiteman, M., Hai, H., Meghji, S.** (2002). Ultrasound stimulates nitric oxide and prostaglandin E2 production by human osteoblasts. Bone, 31, 236–241.

[52] **Fyfe, M., Chahl, L.** (1984). Mast cell degranulation and increased vascular permeability induced by “therapeutic” ultrasound in the rat ankle joint. Br J Exp Pathol, 65, 671–676.

[53] **Lai, J., Pittelkow, M.** (2007). Physiological effects of ultrasound mist on fibroblasts. Int J Dermatol, 46, 587–593.

[54] **Thawer, H., Houghton, P.** (2004). Effects of ultrasound delivered through a mist of saline to wounds in mice with diabetes mellitus. J Wound Care, 13, 171–176.

[55] **Lim, K. T., Cho, C. S., Choung, Y. H.** (2009). Influence of static magnetic field stimulation on cells for tissue engineering. Tissue Engineering and Regenerative Medicine, 6(1–3), 250–258.

[56] **Yun, H. M., Ahn, S. J., Park, K. R.** (2016). Magnetic nanocomposite scaffolds combined with static magnetic field in the stimulation of osteoblastic differentiation and bone formation. Biomaterials, 85, 88–98.

[57] **Zhao, J., Li, Y., Deng, K., Yun, P., Gong, Y.** (2017). Therapeutic Effects of Static Magnetic Field on Wound Healing in Diabetic Rats. Journal of Diabetes Research, ((1-3)), 1–5.

[58] **Henry, S. L., Concannon, M. J., Yee, G. J.** (2008). The Effect of Magnetic Fields on Wound Healing Experimental Study and Review of the Literature. Eplasty, 8, e40.

[59] **Vergallo, C., Dini, L., Szamosvölgyi, Z., Tenuzzo, B. A., Carata, E., Panzarini, E., László, J.** (2013). In Vitro Analysis of the Anti-Inflammatory Effect of

Inhomogeneous Static Magnetic Field-Exposure on Human Macrophages and Lymphocytes. PLoS One, 8(8).

[60] **Zhang, L., Wang, J., Wang, H., Wang, W., Li, Z., Liu, J., Zhang, X.** 2016). Moderate and strong static magnetic fields directly affect EGFR kinase domain orientation to inhibit cancer cell proliferation. Oncotarget, 7(27), 41527–41539.

[61] **Tasić, T., Djordjević, D., De Luka, S., Trbovich, A., Japundžić-Žigon, N.** (2017). Static magnetic field reduces blood pressure short-term variability and enhances baroreceptor reflex sensitivity in spontaneously hypertensive rats. International Journal of Radiation Biology, 93(5), 527–534.

[62] **Brown, C. S., Ling, F. W., Wan, J. Y., Pilla, A. A.** (2002). Efficacy of static magnetic field therapy in chronic pelvic pain: a doubleblind pilot study. American Journal of Obstetrics and Gynecology, 187(6), 1581–1587.

[63] **Darendeliler, M. A., Darendeliler, A., Sinclair, P. M.** (1997). Effects of static magnetic and pulsed electromagnetic fields on bone healing. The International Journal of Adult Orthodontics and Orthognathic Surgery, 12(1), 43–53.

[64] **Gümüşay, M., Gülbağça, F., Aydemir, I., Sayğılı, S., Kaya, A., Tuğlu, M. İ.** (2016). Sıçan Derisinde Oluşturulan Yara Modeli Üzerinde İyileşme Sağlanması için Elektromanyetik Alan Sistemi Geliştirilmesi ve Sensör Uygulaması. EMO Dergisi.

[65] **Shang, W., Chen, G., Li, Y., Zhuo, Y., Wang, Y., Fang, Z., Ren, H.** (2019). Static Magnetic Field Accelerates Diabetic Wound Healing by Facilitating Resolution of Inflammation. J Diabetes Res.

[66] **Davis, S., Ovington, L.** (1993). Electrical stimulation and ultrasound in wound healing. Dermatol Clin, 11(4), 775–781.

[67] **Ennis, W., Foremann, P., Mozen, N., Massey, J., Conner-Kerr, T., Meneses, P.** (2005). Ultrasound therapy for recalcitrant diabetic foot ulcers: Results of a randomized, double-blind, controlled, multicenter trial. Ostomy Wound Manage, 51, 24–39.

[68] **Plonsey R, Collin R. Principles and Applications of Electromagnetic Fields.** (1961). NewYork: Mc.Graw-Hill.

[69] **Zengin R.** (2012). Electrical impedance tomography using Lorentz fields.

[70] **Comsol Modeling Software** (2015). Comsol, Inc.

[71] **Comsol Help Module** (2015). Piezoelectric Material.

[72] **Dunne, E., McGinley, B., O'Halloran, M., Porter, E.** (2018). A realistic pelvic phantom for electrical impedance measurement. Physiological Measurement, 39(3), 0–11.

[73] **Gabriel, C., Gabriel, S., Corthout, E.** (1996). The dielectric properties of biological tissues: I.

[74] **Moran, C. M.** (1995). Original Contribution Propagation Properties of Excised. 5629.

[75] **Wake, K., Sasaki, K., Watanabe, S.** (2016). Conductivities of epidermis, dermis, and subcutaneous tissue at intermediate frequencies. Physics in Medicine and Biology, 61(12), 4376–4389.

[76] **Comsol Help Module** (2015). Acoustics Module Users Guide. epidermis

[77] **JUDI T.WHITTON, J.D.EVERALL** (1973). The thickness of the epidermis. British Journal of Dermatology (1973) 89, 467.

[78] **Koehler M.J., Vogel T., Elsner P., König K., Bückle R., Kaatz M.** (2010). Skin Research and Technology 2010; 16: 259–264.

[79] **Sandby-Møller J, Poulsen T, Wulf HC.** (2003). Epidermal thickness at different body sites: relationship to age, gender, pigmentation, blood content, skin type and smoking habits. Acta Derm Venereol.;83(6):410-3.

[80] **S.I. Alekseev, M.C. Ziskin** (2007). Human Skin Permittivity Determined by Millimeter Wave Reflection Measurements. Bioelectromagnetics 28:331-339.

[81] **Jacques L S., Prahl A S.** (1987). Angular Dependence of HeNe Laser Light Scattering by Human Dermis. Lasers in the Life Sciences 1(4),1987, pp. 309-334.

[82] **Huang H., Guo Z.** (2009). Human dermis separation via ultra-short pulsed laser plasma-mediated ablation. J. Phys. D: Appl. Phys. 42 (2009) 165204 (9pp).

[83] **Lai-Cheong J., McGrath J.** (2021). Structure and function of skin, hair and nails. BASIC SCIENCE— VOLUME 49, ISSUE 6, P337-342.

[84] **Sachs D., Wahlsten A., Kozerke S., Restivo G., Mazza E.** (2021). A biphasic multilayer computational model of human skin. Biomechanics and Modeling in Mechanobiology (2021) 20:969–982.

[85] **Stremitzer S., Wild T., Hoelzenbein T.** (2007). How precise is the evaluation of chronic wounds by health care professionals. Int Wound J 2007;4:156–161.

[86] **IMASONIC** Phased Array Probe Specifications.

[87] **Zhou C, Zhang B, Yang Y, Jiang Q, Li T, Gong J, Tang H, Zhang Q.** (2023 Apr 26). Stem cell-derived exosomes: emerging therapeutic opportunities for wound healing. Stem Cell Res Ther.;14(1):107

[88] **Zhao, M., Song, B., Pu, J. et al.** (2006). Electrical signals control wound healing through phosphatidylinositol-3-OH kinase- and PTEN. Nature 442, 457–460.

[89] **Burgess RC.** (2019). Electrical safety. Handb Clin Neurol. 160:67-81.

[90] **Lionheart WR, Kaipio J, McLeod CN.** (2001). Generalized optimal current patterns and electrical safety in EIT. Physiol Meas. Handb Clin Neurol. 22(1):85-90.

[91] **Farber PL, Isoldi FC, Ferreira LM.** (2021). Electric Factors in Wound Healing. Adv Wound Care (New Rochelle) 10(8):461-476.

[92] **Carley, P., S. Wainapel, P. J. Carley, and S. F. Wainapel.** (1985). Electrotherapy for acceleration of wound healing: low-intensity direct current. Arch. Phys. Med. Rehabil 1985; 66:443–446.

[93] **Feedar, J. A., L. C. Kloth, and G. D. Gentzkow.** (1991). Chronic dermal ulcer healing enhanced with monophasic pulsed electrical stimulation. Phys. Ther 1991; 71:639–649.

[94] **Jankovic, A., and I. Binic.** (2008). Frequency rhythmic electrical modulation system in the treatment of chronic painful leg ulcers. Dermatol. Res 2008; 300:377–383.

[95] **Magnoni, C., E. Rossi, C. Fiorentini, A. Baggio, B. Ferrari, and G. Alberto.** (2013). Electrical stimulation as adjuvant treatment for chronic leg ulcers of different etiology. An RCT. J. Wound Care 2013;22:525–533.

[96] **Gault, W. R., and P. F. Gatens.** (1976). Use of low-intensity direct current in management of ischemic skin ulcers. Phys. Ther. 1976; 56:265–269.

[97] **ICNIRP STATEMENT** (2009). Amendment To The ICNIRP "Statement on Medical Magnetic Resonance (MR) Procedures: Protection of Patients". Health Physics 97(3):259-261.

[98] **Rentech** (2013).https://www.rentech.com.tr/urun/helmholtz-bobinleri-deney-seti-vernier-versiyon-2/

[99] **Azhari H.** (2010).Basics of Biomedical Ultrasounds for Engineers: A John Wiley and Sons, Inc., Publication.

[100] **Lionheart WRB, Kaipio J, McLeod CN.** (2001). Generalized optimal current patterns and electrical safety in EIT. Physiological Measurement. 22:85.

[101] **Konstantinou, E., Z. Zagoriti, A. Pyriochou, and K. Poulas.** (2020). Microcurrent stimulation triggers MAPK signaling and TGF-1 release in fbroblast and osteoblast-like cell lines. Cells. 9:1924.

[102] **Merriman, H. L., C. A. Hegyi, C. R. Albright-Overton, J. Carlos, R. W. Putnam, and J. A. Mulcare. A** (2004). Comparison of four electrical stimulation types on Staphylococcus aureus growth in vitro. J. Rehabil. Res. Dev. 41:139.

[103] **Bourguignon, G. J., and L. Y. W. Bourguignon.** (1987). Electric stimulation of protein and DNA synthesis in human fbroblasts. FASEB J. 1:398–402.

[104] **rabbani m, rahman e, powner mb, triantis if.** (2024). making sense of electrical stimulation: a meta-analysis for wound healing. ann biomed eng. 52(2):153-177

RESUME

Aliye GÜRCAN

EDUCATION STATUS :

- **Bachelor Degree :** 2021, INONU UNIVERSITY, ENGINEERING FACULTY, DEPARTMENT OF BIOMEDICAL ENGINEERING
- **Master :** 2024, INONU UNIVERSITY, ENGINEERING FACULTY, DEPARTMENT OF BIOMEDICAL ENGINEERING

PROFESSIONAL EXPERIENCE:

July 2024-... Zimed Medikal, Biomedical Department, GAZİANTEP.

July 2023- July 2024-Türev İç ve Dış Ticaret A.Ş., Biomedical Department, GAZİANTEP.

March 2022- September 2022-Breegi Technology Company, R&D, MALATYA.

STUDIES DERIVED FROM MASTER'S THESIS (Articles, Papers, Patents, etc.)

- A. Çalış and R. Zengin, "NON-SURGICAL WOUND HEALING METHODS", December 2023, International Research in Health Sciences
- M. Kömür, A. Gürcan, and R. Zengin, "A NOVEL WOUND HEALING METHODS USING LORENTZ FIELDS", May 2024, EWMA
- A. Gürcan, M. Kömür, R. Tutuk, E. Aydın, and R.Zengin, " EXPERIMENTAL STUDIES ON A NOVEL WOUND HEALING METHOD USING LORENTZ FIELDS", March 2025, EWMA